



k People's Democratic Republic of Algeria
Ministry of Higher Education and Scientific
Research SAAD DAHLEB University of Blida
Institute of Aeronautics and Space Studies



END OF STUDY THESIS FOR OBTAINING THE MASTER'S DIPLOMA

Specialty: aircraft propulsion

Option : PROPULSION

**THEME: SIMULATION OF FLOW IN PLUG
NOZZLES**

Framed by :

MR KBAB HAKIM

MR HAIF SIDALI

Realised by :

TAILBA AMIRA

Presented in front of the juries

MR HERTSI ABDELLAH

MR OULD BESSI HAMID

Academic year: 2022/2023



*First of all, we thank "ALLAH" the Almighty, who gave me the Power, the will and the patience to develop this work. I would like to thank **Mr KBAB HAKIM** our supervisor and my Co-promoter **Mr HAIF SIDALI** for having agreed to lead us on this little path of a great experience, and for having been passionate with us even with all the troubles we have. caused him and for his valuable advice and constructive criticism which guided this modest research work to its conclusion.*

A big thank you for all the personnel of the aeronautics department who gave effort, For us and for our best.

I would like to express my deep gratitude to all my family and to all those who have contributed directly or indirectly to the realization of this work. They are warmly thanked.

Dedication

*I dedicate this work, which is the fruit of a lifetime of study: To those who made my existence possible, to those who sacrificed their lives for my happiness, my dear parents, my father **AEK** and my mother **DEBOUCHE Samira**. To those who are closest to me, who have always shared my good and my bad with me, my brother **Ayoub** and my sister **Aya**, to my great mother **BENKAHLA Malika** who has helped me and who continues to help me morally and physically without forgetting to the one who, by their friendship, by their orientations, their support and their comments, have often pushed me to clarify and deepen many points treated here in particular my dear tents and my uncle **Nordine** and my companions in life, supported me during my defeat my dear friends name by name and person by person.*

Summary

This work consists in simulating a flow through a CENTRAL BODY nozzle based on a CD nozzle using a CD simulation tool. This simulation took place in four phases (Creation of the surface geometry, Mesh of the geometry, Resolution and Visualization of the Results), it is based on the parametric analysis (Number of Mach, Static Pressure and Density) in the configuration (Perfect gas).

SOMMAIRE

Ce travail consiste à simuler un écoulement à travers une buse CENTRAL BODY basée sur une buse CD à l'aide d'un outil de simulation CD. Cette simulation s'est déroulée en quatre phases (Création de la géométrie surfacique, Maillage de la géométrie, Résolution et Visualisation des Résultats), elle est basée sur l'analyse paramétrique (Nombre de Mach, Pression Statique et Densité) dans la configuration (Gaz parfait).

ملخص

يتكون هذا العمل من محاكاة التدفق عبر فوهة CENTRAL BODY بناءً على فوهة CD باستخدام أداة محاكاة القرص المضغوط. تمت هذه المحاكاة على أربع مراحل (إنشاء هندسة السطح، وشبكة الهندسة، والدقة وتصور النتائج)، وهي تستند إلى التحليل البارامتري (عدد الماخ، والضغط الثابت، والكثافة) في التكوين (الغاز المثالي).

TABLES DES MATIERES:

Thanks	
Dedication	
Summary	
Table of materials	
Nomenclature	
List of figures	
List of tables	
General introduction	1
CHAPTER I STATE OF ART AND DEFFINITIONS	3
Bibliography	4
I-1/nozzle definition	4
I-2/Introduction of the supersonic nozzle	4
I-3/various types of nozzles	4
I-3-1/conventional nozzles	4
I-3-2/innovative nozzles	7
CHAPTER II PERFORMANCES	12
I/ performances setting.	13
II/ different operating mode nozzles	15
CHAPTER III SIMULATION OF SUPERSONIC FLOWS IN NOZZLES	18
I/Introduction	19
II/ANSYS and fluent	20
III/fluid mechanics equations	22
IV/mean equation motion	23
V/different types of rivers	25
VI/turbulence pattern	27
VII/traditional numerical methods in CFD	29
VIII/discretization of computational domain	31
IX/comparaison between structured and unstructured mesh	34

X/conclusion	35
CHAPTER IV RESULTS	36
Introduction	37
I/ I/ 16-FOOT TRANSONIC TUNNEL (BUILDING 1146)	38
II/ TEST NOZZLE	40
II-1/ Flow visualization	41
II-2/ Experimental results	42
III/ NUMERICAL SIMULATION	42
III-1/ geometry	43
III-2/ meshing	44
III-3/ configuration	47
III-4/ RESULTS	49
III-4-1/ Validations	49
III-4-2/ Simulation 2D	50
III-4-3/Contour of Mach:	53
III-4-4/Thrust coefficient	55
IV/ OPTIMIZATION OF THE NOZZLE	57
IV-1/ geometry	58
IV-2/ Results	59
IV-2-1/Contour of mach	62
IV-2-2Thrust coefficient	63
IV-3/ COMPARAISON	64
IV-4/ TRUNCATION OF THE CENTRAL BODY	67
V/NOZZLE PERFORMANCES	70
VI/CONCLUSION	73

Nomenclature :

I. LATIN LETTERS

Pa : Ambient pressure

CP: : thrust coefficient

M : Mach number

Ms : ejection Mach number

Cp : pressure coefficient

μ : Dynamic viscosity

U : Velocity (Vitesse) , m/s

T : Temperature, K

P : Pressure, Nm⁻²

X : : axial distance ,

m a : Speed of sound

P/P0 : Ratio of static pressure to initial pressure

L : length, m

P : thrust

Cb: central body

II. INDEX

C col

E nozzle outlet

\bar{x} Average value.

\acute{x} Fluctuating value.

Δ Gradient operator.

Δ . Divergence operator.

\mathbf{x} Value at the speed of sound

∂ Partial derivative

Π_{geo} Geometric yield.

III.FIGURES LIST

Chapter I : state of art and definitions

Figure I. 1: laval nozzle.....
Figure I. 2: conical nozzle
Figure I.3 variable cross section nozzle
Figure I. 4: duall bell nozzle.....
Figure I. 5:adjustable nozzle
Figure I. 6: : rétractable déflexion nozzle

Chapter II : performances

Figure II. 1: evolution of the cd according to the geometry.....
Figure II. 2: regime subsonique.....
Figure II. 3: Ecoulement sonique adapté.....
Figure II. 4: Ecoulement sonique non adapté.....
Figure II. 5: Régime supersonique adapté.....
Figure II. 6: Régime supersonique non adapté.....

chapter III: Simulation of supersonic flows in nozzles

Figure III. 1: laminar flow and turbulant flow
Figure III. 2 : Control volume in a three-dimensional configuration.....
Figure III. 3: illustration of the concept of mesh.....
Figure III. 4: Structured mesh for nozzles.....
(a multi-block, b mono-block)
Figure III. 5: hybrid unstructured network

chapter VI : RESULTS

FigureIV.1: : Overexpanded CD Nozzle with Separation

FigureIV.2: Nozzle Flap Geometry

FigureIV.3: Test Nozzle

FigureIV.4: : Experimental Centerline Pressure Data

FigureIV.5: geometry

FigureIV.6: unstructured mesh on top of a refined mesh.

FigureIV.7: Create a named selection.

FigureIV.8: statistiques

FigureIV.9: calculation model

FigureIV.10 The evolution of pressure as a function of different NPRs compared to the experimental results

FigureIV.11: geometry

FigureIV.12: comparaison ofpression wall1 and 2 for npr =1,255

FigureIV.13: comparaison ofpression wall1 and 2 for npr= 2,008

FigureIV.14: comparaison ofpression wall1 and 2 for npr=2,412

FigureIV.15: comparaison ofpression wall1 and 2 for npr=3,816

FigureIV.16: comparaison ofpression wall1 and 2 for Npr=5,423

FigureIV.17: contour of iso-machfor Npr=1,255

FigureIV.18: contour of iso-machfor Npr= 2,412

FigureIV.19: contour of iso- machfor Npr=3,816

FigureIV.20: contour of iso-machfor Npr=5,423

FigureIV.21: cp as a function of npr

FigureIV.22: geometry

FigureIV.23: p/po as function of x for npr=1,255

FigureIV.24: p/po as function of x for npr=2,214

FigureIV.25: p/po as function of x for npr=3,816

FigureIV.26: p/po as function of x for npr=5,423

FigureIV.27: p/po as function of x for npr=4,620

FigureIV.28: contour of iso-machfor npr=1,255

FigureIV.29: contour of iso-machfor npr=2,412

FigureIV.30: contour of iso-machfor npr=3,816

FigureIV.31: contour of iso-machfor npr=4,620

FigureIV.32: contour of iso-machfor npr=5,423

FigureIV.33: cp as a function of npr

FigureIV.34: p/po as a function of x for npr=1,255

FigureIV.35: p/p_o as a function of x for $npr=2,412$

FigureIV.36: comparaisn

figure IV.37 Schematics of side load due to unsymmetrical flow separation

Figure IV.38 Side load variation with respect to NPR for two nozzles

FigureIV.39: geometry at 20% of the cb

Figure IV.40 geometry at 40% of the cb

FigureIV.41: $p[pa]$ function of $x[m]$

FigureIV.42: $p[pa]$ function of $x[m]$

FigureIV.43: $p[pa]$ function of $x[m]$

FigureIV.44: $p[pa]$ function of $x[m]$

FigureIV.45: Thrust coefficient function of npr

Figure IV.46 :weight gain/loss at truncated points

IV. LIST OF TABLES:

Tableau III.1 COMPARAISON BETWEEN turbulence models

Tableau III.2 structured and unstructured mesh.....

GENERAL INTRODUCTION:

Gas expansion and exhaust in various propulsion systems, such as jet engines and rockets, always occurs through nozzles. The thrust of a conventional fixed-geometry nozzle discharging into the atmosphere can be expressed by the following simple relationship: $F = \dot{m} V_e + (P_e - P_a) A_e$, where F is thrust, \dot{m} is mass flow rate, V_e is exit velocity, P_e is exit pressure, P_a is ambient pressure, and A_e is exit area. Thrust is affected by changes in altitude. At the design altitude where $P_{atm} = P_{des}$, the second term in the above relationship (known as the pressure stroke) is zero and the nozzle is operating "optimally". At altitudes below the design altitude where $P_{atm} > P_{des}$, pressure thrust becomes negative and thrust loss is inevitable. These conditions, which occur at heights above ground level to the design elevation, are called "overstretched" conditions. In addition to the inherent loss of thrust, conventional nozzles can suffer from other problems such as shock wave and flow separation in the divergent section, thrust oscillations and flow asymmetry under hyper expansion conditions.

Since the advent of jets and rocket propulsion systems, researchers have invented and implemented many types of jets. Among these various designs, the characteristics of the center body nozzle (specifically known as the plug nozzle) have been the subject of research since the mid-1950s

Many theoretical studies on central body nozzles were carried out in the 1960s. The work of Berman and Crimp is an example of such work, with analytical design methods, thrust vectorization, solid and liquid It deals with issues such as the integration of A propellant system was discussed. Rao [54] presented a more accurate method based on variational calculations for the central body (The Plug) design in 1961, and Lee and Thompson [55], based on Rao's work, proposed a plug nozzle design in 1964. Developed the first computer program for , the heat and strength issues of central body nozzles, and the development of more efficient methods of manufacturing conventional nozzles, have reduced research activity in this area.

In the 1990s, NASA launched his SSTO (Single Stage to Orbit) project. This required a propulsion system with maximum efficiency at a wide range of working altitudes. For this purpose, a central body propulsion system was selected, extensive research and

The development resulted in a successful test of the RS2200 Aerospike engine Although the discontinuation of this project in 2001 has further reduced research activity in the field in the United States in recent years, central body his jet remains an active research subject in Europe and Japan. Hagemann et al. proposed the use of a large-area aerospike nozzle for the DLR's Ariane 5 launch vehicle. Tomita et al. and Sakamoto et al. conducted experimental studies on axisymmetric and linear central body nozzles, and Fujii and Ito investigated many aspects of the central body nozzle numerically. Recently, two different groups of his in the United States used an axisymmetric central body nozzle for observations of the rocket propulsion system

Central body nozzles have the best overall performance compared to traditional bell nozzles because the jet spread is not restricted by walls and the exhaust flow can be adapted to the environment by changing the jet restriction will demonstrate. Furthermore, it is assumed that the nozzle performance is not affected by the latter clipping, as the exit pressure compensates for the loss of thrust. Outlet pressure can also be increased by injecting a secondary flow at the outlet. It can be obtained from the exhaust gas stream and injected [63]. See reference [64] for a detailed off-design performance comparison of midbody and conventional nozzles.

The work performed in our paper consists of simulating and analysing the flow in the central body nozzle and studying its effect on the nozzle performance. Simulations run on Ansys 19. Evaluations of thermodynamic parameters (Mach number, static pressure, static temperature, etc.) are analysed.

STRUCTURE OF THE PROJECT:

A survey of the issues considered is done in four chapters and a general conclusion.

The first chapter contains a detailed literature survey on various nozzles. Various profiles of conventional nozzles are shown. Finally, we present different nozzle configurations with height compensation.

Chapter 2 focuses on performances and their definitions. Chapter 3 is about simulation of supersonic flow in nozzles ,

The final chapter is devoted to the presentation of all results obtained with the ANSYS 19 software and the interpretation of the obtained parameters (Mach number, pressure and temperature).

The work ends with a general conclusion summarizing the aims of this work and the main results obtained. Prospects for continuing this research are proposed.

Chapter I :

State of the art

And

Definitions

BIBLIOGRAPHY:

Nozzle is a variable area tube attached to the rear of the engine that produces hot combustion gases and converts thermal energy into kinetic energy. The principle of operation of the nozzle is based on the properties of gases circulating at subsonic and supersonic speeds. As the gas flows subsonic in a pipe of decreasing diameter, its velocity increases. Over the years, the work of several researchers in this field has enabled numerical, analytical and experimental solutions to aerodynamic problems such as liquid flow in convergent-divergent nozzles.

After World War II, jet research became an area of current competition and competition between the United States, the European Union, Russia, Japan and China. Several program agencies (ESA, CNES, CNSA), research institutes (NASA, ONERA, NASDA, DLR, LEA-Poitier), industry associations (Boeing, Rocketdyne, Pratt & Whitney, Snecma Motors, Volvo Aero, Astrium, Mitsubishi Heavy Industries) are working to improve the performance of rocket engines and fuel nozzles.

Rocket nozzles come in a variety of configurations that have been developed over the last 75 years. Examples include ideal, conical, bell, plug, extended deflection (E-D), double bell and even the recently developed multi-nozzle grating (MNG). This chapter provides an overview of the research done in this area.

I.1: Nozzle Definition

Nozzles play a crucial role in propulsion systems as they are responsible for converting the thermal energy of hot combustion gases into kinetic energy. Positioned at the propellant exit, these variable-section chimneys facilitate the expansion of combustion gases, resulting in a significant increase in the spacecraft's ascent into space. By efficiently harnessing the energy of combustion, nozzles propel the spacecraft forward and contribute to its successful journey beyond Earth's atmosphere.

I.2: Introduction of the supersonic nozzle

The supersonic spout may be a converging-diverging conduit with a uncommonly examined profile. It interfaces a chamber containing compressed gas to an outside deplete medium. The chamber and the outside environment are at diverse weights to permit gas development. The part of the supersonic spout is to quicken the gas from moo speed at the focalized entrance to sonic speed at the throat and supersonic speed at the unique exit. Gas

speed increments along the spout and weight and temperature diminish. Supersonic spouts are called Laval nozzles.

Hypothetical Usefulness of Supersonic Spouts

1.3 various types of nozzles

1.3.1 Conventional nozzle

a. Conical nozzle

Nozzles with a conical profile are mainly used for design simplification and divergence. The exit velocity of this type of nozzle is essentially a value corresponding to the one-dimensional expansion rate, except that the flow direction at the exit is not exactly axial, resulting in power loss due to flow divergence. The divergence angle is between 15 and 25 degrees. This type of basic profile will be primarily equipped with rockets and rocket boosters. An example of a conical nozzle is that of the historic German V-2 rocket.

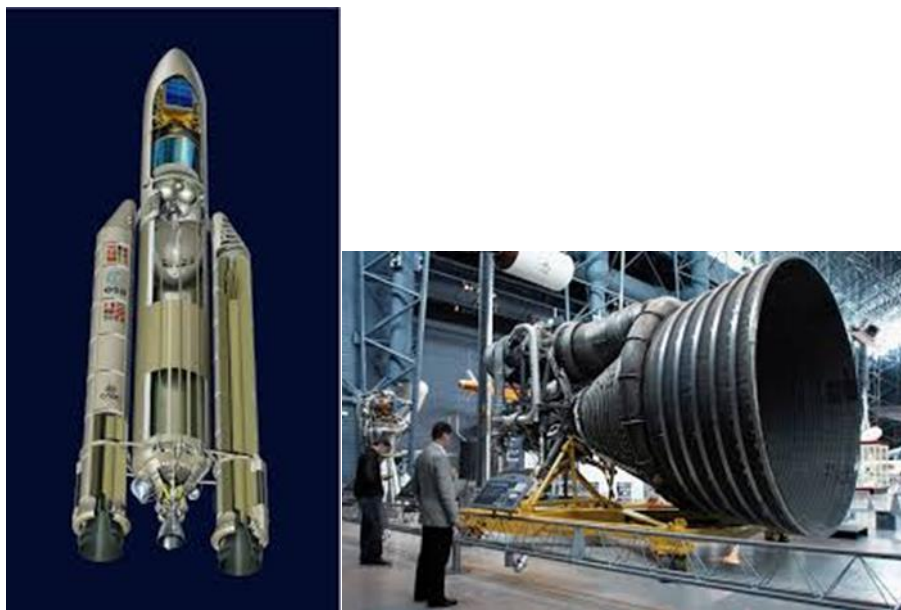


Figure (I.2) : Conical nozzle

The use of tapered nozzles was very common in early rocket engines. The main advantage of conical nozzles is their ease of construction and the ability to convert existing designs to lower or higher area ratios without major modifications. Best performance for this type of nozzle is achieved with a divergence angle of 15. The thrust coefficient of the 15 conical nozzle is only 1.7% lower than that of the ideal nozzle and varies slightly with altitude. As a result, the performance and length of new nozzles are of Carl Gustav Patrick de Laval developed the convergent-divergent (CD) nozzle in 1890 with the ability to make the steam jet supersonic

This nozzle is called a Laval nozzle. From the late 1930s to his early 1940s, extensive research on various profile his types was carried out by German scientists. After considering all aspects of the design, they found that there were no significant advantages to justify the use of

complex outlines. However, this statement only applies to low aspect ratio nozzles like his V2 rocket. In 1963 Darwell and Badham [3] performed a numerical study on conical nozzles. Using the characteristic curve method, they were able to show that the formation of impulses in the nozzle can be eliminated by altering the profile of the groove and the wall near the junction of the cone. In 2008, Khan and Shembharkar [4] performed numerical studies using a computational fluid dynamics (CFD) computer code. They successfully visualized the flow in a convergent-divergent (CD) nozzle. High-flow conditions were examined, allowing for the determination of the impact location and detachment point. The findings demonstrated that an increase in the Nozzle Pressure Ratio (NPR) resulted in a displacement of the impulse towards the nozzle exit. In a study conducted by Balabel et al. [10] in 2011, turbulence was investigated in a two-dimensional (2D) convergent-divergent (CD) nozzle.

The relevant physical phenomena were analyzed under various operating conditions. The results showed that the viable v^2 -f model and the KW-SST model performed better than the other models in predicting the separation point and shock wave location. In 1965, Hoffman and Lorenc conducted a numerical study on the effects of his 2D gas particle flow in a conical nozzle. In 1970, Wehofer and Moger [8] developed an analytical method for studying inviscous transonic flow fields in connection with convergent-divergent (CD) and convergent conical nozzles. In 2015, Jia et al. numerically demonstrated the effects of a fire event in the borehole on initiation flow separation and lateral loading of a conical nozzle in flight. A year later, they again performed a numerical study on three-dimensional (3D) side loads. In 1964, Sunley and Ferriman conducted tests to study jet separation in conical nozzles. They showed that the pressure at which the gases separate is not constant and independent of nozzle length.

b .bell nozzles

Bell nozzles are the most common shape used in rocket engines. Nozzles in this category offer significant performance and size advantages compared to conical nozzles. It features a wide angle (20-50) flare section just behind the nozzle throat. This is followed by a gradual reversal of the slope of the nozzle profile and a smaller divergence angle at the exit, preferably less than 10.

As we have seen, conical nozzles suffer a significant loss of thrust due to flow divergence at the exit. So this issue should be resolved. The divergence profile should be turned inward to return the flow axially, transitioning to a relatively significant divergence value in the divergence part near the throat, and tilting the profile inward to compensate for the lack of relaxation. Interior space is the purpose of this design.

In 1957, Dillaway analytically calculated the nozzle exit profile by gradually decreasing the slope of the nozzle wall, from which he concluded the dependence of the flow on the nozzle profile. In 1960, according to Lands Baum [17] a variety of ideal stubs with different aspect ratios, he analysed nozzles and suggested choosing the one that gave the best performance. In 1960, Farley and Campbell investigated an ideal truncated nozzle experimentally. The results obtained are very close to the theoretical values. In 1961, Hallberg et al. A graphical method that allows you to select the best nozzle profile from a family of disconnected nozzles. In 1958, Rao developed a method for designing optimal nozzle contours using variational calculus.

In 1981, Allman and Hoffman reviewed techniques for designing nozzle contours at maximum thrust using direct optimization techniques. The nozzle contour was given by a second order polynomial. The authors compared shear forces generated by variational contour calculations (Raos method) with those generated by polynomial contours. They concluded that both methods predict essentially the same maximum thrust.

In 2017, Frey et al. [31] presented a new nozzle contour technique called TICTOP. This method combines a shortened ideal contour design (TIC) and an optimized thrust parabolic design (TOP). The results obtained indicate that the nozzle does not exhibit shock and cause flow separation leading to large lateral loads. The pressure obtained at the outlet is superior compared to the profile (TOP). In 2004, Pilinski and Nebbache [26] numerically analyzed the flow nozzle separation at various NPRs in the nozzle (TIC). Free shock separation (FSS) was measured for very low and high pressure ratios. Between these two pressure ratio ranges, shock occurred without reattachment. In 2006, Verma et al. conducted a series of tests on TOP nozzles to investigate the relationship between the transient characteristics of delamination and reattachment shocks and the sources of lateral loading of the nozzle. Another experimental study was performed to identify the causes of various flow conditions that lead to the generation of side loads in TIC nozzles.

In this study, changing the circumferential geometry of the recirculation section within the nozzle from a cylindrical dominant region to a conical and final effect region leads to highly unstable flow conditions in the separation region prior to these transitions. It is concluded that it is caused by In 2002, Hagemann et al. stated:

To investigate the causes of different side loads, he tested two different nozzle types against the same performance data: an optimized exhaust nozzle and an ideal truncated cone nozzle. The results showed that the highest lateral loads occurred in the thrust-optimized nozzle when changing the separation pattern from free impact separation to constrained impact separation. The measured side load for the ideal frusto-conical nozzle was only about 33.33% of the side load for the thrust-optimized nozzle. In 2017, Baloni et al. [32] performed his two-dimensional axisymmetric flow study in a streamlined nozzle under off-design conditions using the CFD software Fluent 6.3.26 and GAMBIT 2.4.6. Numerical simulations were performed separately for two different flow conditions, hot and cold. In 2006, Stark and Wagner [30] performed tests aimed at analysing the nozzle flow field (TIC).

Low NPR value. They found that the Mach disc has a convex shape at his NPR values below 10 and a concave shape at his NPR values above 20 .

In 2009, they investigated boundary layer separation and associated flow fields in his TIC nozzle. In 2017, Zhang et al. quantified the aeroelastic stability of rocket nozzles during launch. They concluded that the aeroelastic behaviour of rocket nozzles is highly dependent on wall thickness and wall material properties.

1.3.2: innovative nozzle

a: variable cross section nozzle

The nozzle exit has a variable cross-section and consists of a number of flaps that are moved closer together or further apart to change the diameter of the nozzle and "tune" it. To make it as close to circular as possible, half bolts are produced by a number of small flaps that fit together. Position control is generally ensured by a ring being pulled or pushed (open and closed) by cylinders placed around the post-combustion duct. The pressure and velocity of the jet keep the flaps pressed against the control ring. Locating lugs prevent flaps from lowering when the engine is off.

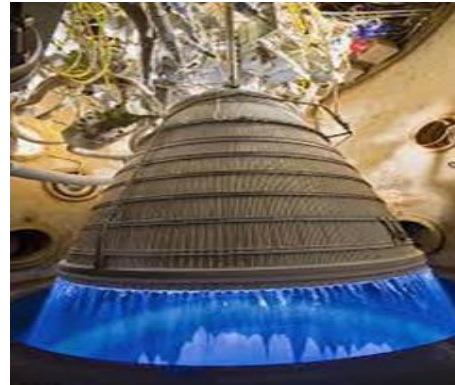
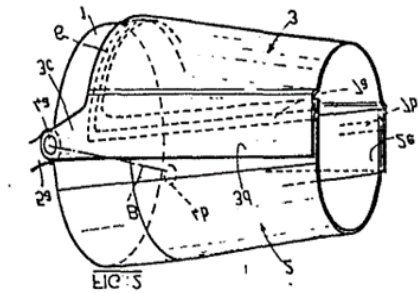


Figure (I.3) :Variable cross section nozzle

plug Nozzle

The central body nozzle is an advanced rocket nozzle consisting of a relatively conventional shaped primary nozzle and a plug that allows for external expansion. A key feature of this nozzle is its interaction with the external environment, which avoids the delamination phenomenon that occurs with conventional profile nozzles. These benefits come from forming an expansion fan on the lip of the primary nozzle and its influence on the development of pressure along the plug wall

. In 1961, Berman and Crimp compared conventional nozzles and plug nozzles. The results show that the plug nozzle outperforms the conventional nozzle when operated at lower pressure ratios than designed. This is because the nature of the flow in this case is self-regulating. In 2002, Ito et al. [41] Plug nozzle flow field using numerical simulations. They considered different types of plug nozzles by using the feature method to design the plug contour and shortening the nozzle length at different positions. As a result, compared with the conical plug nozzle, the thrust performance of the contour plug nozzle was improved by about 5-6%, and it was found that the pressure distribution on the nozzle surface was not affected by the external flow at pressure ratios exceeding the design point. In 2006, Shahroghi and Noori [44] studied the flow properties of various aerospike nozzle profiles using the k- ϵ turbulence model and standard Navier equations for flow field simulation. A uniform cubic B-spline curve was used to generate various connector shapes. The optimal configuration was determined by considering total thrust as a performance characteristic. In 2002, Besnard et al. [42] designed, built and tested a 1000 lb thrust annular aerospike ablation engine. Results show that changes in γ with temperature produce small, if not zero, differences in thrust characteristics. Moreover, this nozzle has proven to be very effective. In 2002, Lahouti and

Tolouei [43] numerically modelled the external and internal flows of a truncated cone nozzle with several basic venting stages under -, optimal, and over-expansion operating conditions. Executed. Extensions to get basic jet thrust, basic pressure distribution and flow patterns. 2015, Shanmuganathan et al. [46] conducted a study on linear and annular aerospike nozzles and their flow field properties. They found the annular aerospike nozzle to be superior to the linear aerospike nozzle. In 1997, Ruf and McConnaughey [40] found that shortening the plug nozzle by 50° reduced performance by 0.5°. A larger taper angle can be used at the end of the cap to avoid flattening the top of the cap after trimming. In 1961, Rao [37] developed a numerical study of typical optimal crown contours. The length of the nozzle can be shortened by using a plug.

C: dual bell nozzle

The main purpose of double curved nozzles is to improve performance through the principle of self-adjustment to altitude. In fact, the system has the advantage of being able to automatically adjust the flow in two operating conditions (low and high altitude) without the need for mechanical actuation. The principle is very simple in theory, but structurally it can be quite labour intensive. This allows us to thoroughly study this concept in order to ensure optimal operation of this system.

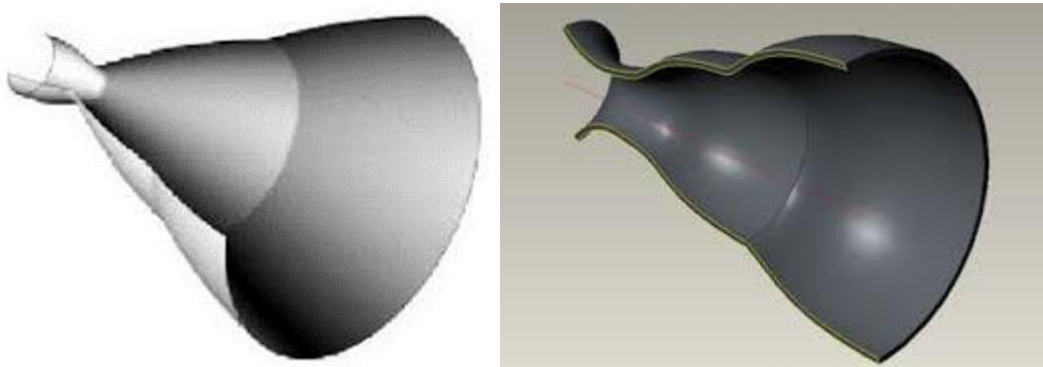


Figure (I.4) :dual bell nozzle

Double curved nozzles are considered a solution to maximize efficiency at high altitudes and avoid dangerous side loads at low altitudes. The dual curve nozzle consists of two different profiles, the first intended for low altitude use and the second for high altitude use. These two contours are separated by a connection point

In 1949 Cowles and Foster [2] introduced the concept of a double curve nozzle. This concept he patented by Rocket Dyne in the 1960s. In 1994 Horn and Fischer [58] confirmed the feasibility of this nozzle by conducting tests in Europe with Rocketdyne as part of the future European Space Transportation Research Program. European Space Transportation Survey (FESTIP). They considered four profile combinations and found the extension that provided the most favorable flow transition characteristics and best high altitude performance. Double curved nozzles have been shown to perform below the theoretical optimum due to drag-related losses in low flight modes and non-optimal contours in high flight modes. They found that even

with such losses, the twin-bell nozzle could still provide enough thrust to carry 12.1 additional payloads compared to a conventional CD nozzle with the same expansion rate

In 1999, Frey and Hagemann [59] studied various aspects of wall deflection and nozzle extension design, focusing on the dependence of transient behaviour on nozzle extension type. In 2013, Genin et al. conducted experimental and numerical studies on double curved nozzles to evaluate the heat flow distribution. They showed that both modes of operation (sea level and altitude) resulted in increased heat flux values in regions of contour curvature. This phenomenon is exacerbated when the flows separate at bends. Under sea level conditions, the currents separate in contour curves in a controlled and symmetrical manner. Due to the low area ratio, lateral loads generated continue to decrease and thrust increases. During flight, ambient pressure decreases and NPR increases. At a certain height the NPR transition is reached, and the split point leaves the contour bend and moves rapidly towards the nozzle exit. The larger the surface area ratio, the higher the thrust. They also tested a model of a double bend flat nozzle under various test conditions in cold flow and hot flow. Impact analysis at contour turning points provided information on the shape and position of the detachment front. For the sea level mode, the numerical and experimental results agree well at higher NPR values, and the calculated splitting positions were further upstream than those measured in the experiments. In 2016, Schneider and Genin [70] analysed the effects of different turbulence patterns and supply pressure gradients on the flow transition behaviour of double curvilinear nozzles. They found better results for Reynolds stress turbulence and SpalartAllmaras models. In 2013, 2014 and 2015, Verma et al. [66], [67], [69] conducted his three experimental studies.

In 2005 and 2012, Chasman et al. [74], [75], [76] conducted three experimental studies on multi-curve nozzles (MNG). The first study explored multidisciplinary optimization (MDO) to design innovative multi-curve configurations. In a second step, a hot firing test of 91 He MNG-configured nozzles featuring very high nozzle erosion at an average velocity of 0.5 lbs/sec was performed. In a third step, he studied the viscosity loss of MNG when testing hybrid engines. . Viscosity loss in the flow through the MNG resulted in a 3% reduction in efficiency compared to that of a comparable single nozzle (ESN). Here it is worth mentioning that a single nozzle with the same scale nozzle profile and the same overall throat and exit areas is called ESN. The MNG system can improve performance by more than 11% due to weight and length savings.

d.adjustable nozzle

It is a nozzle articulated about one or two axes, consisting of a fixed part on the one hand, an articulated part and a control cylinder on the other, allowing the articulated part to move and an elastic ring structure. You can move the axis by transforming it. align the thrust



Figure (I.5) :*adjustable nozzle*

E: retractable deflection nozzle

The nozzle has a longitudinal axis and has a first portion defining a nozzle throat, a first fixed diverging section and at least one second deployable diverging section having a larger cross section than the first section. and a mechanism for deploying a second section located thereon. The outside diverges the first section and his second section. The deployable portion of the Divergent is automatically triggered by electrical, hydraulic, or pneumatic controls.

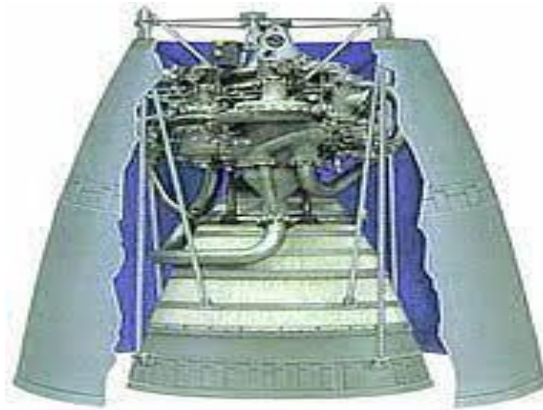


Figure (I.1) :*rétractable déflection nozzle*

Chapter II :

Šrón Āl'sē

I: Performance settings

I.1: The thrust

It is the force provided by the nozzle which is a function of the gas ejection speed and the flow rate passing through it. It is described by the relation

$$F = mV_e + (P_e - P_0) \dots\dots\dots(\text{II.1})$$

V_e : ejection velocity.

P_e : Outlet pressure.

P : Ambient pressure.

I.2: The thrust coefficient

It is a dimensionless entity representing the ratio of the thrust to the product of the pressure generated and the Nozzle exit area, which characterizes the performance of the divergent or the quality of inflation of the divergent

$$C_F = \frac{F}{P_t S_c} \dots\dots\dots(\text{II.2})$$

F : Thrust force;

P_t : Total pressure;

S_c : Outlet section of the nozzle.

I.3: runoff coefficient

If we assume that the liquid is a perfect liquid with no viscosity, or that the flow is isentropic, this is only to simplify the calculations and the equations describing general phenomena in aerodynamics and fluid dynamics. It's just However, in practice this is not true, as this assumption quickly introduces error into the results. To fix this, the latter introduces the flux coefficient, a dimensionless unit that represents the error introduced by each unit of the result.

$$Cd = \frac{\text{Débit actuel réel}}{\text{Débit actuel isentropique}} \dots\dots\dots(\text{II.3})$$

The figure below shows the evolution of the coefficient Cd according to these parameters:

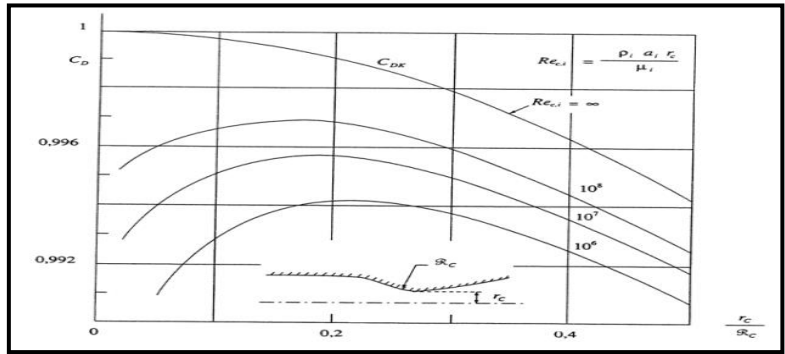


Figure (II.1) :: Evolution of the coefficient Cd according to the geometry.

I.4: The characteristic speed

It is the speed measured at the level of the ring marked C* and is often used to represent the speed in the whole of the pipe or more particularly in the nozzle, according to the properties of the fluid and the temperature at which it is produced

$$C = P_t/m \dots\dots\dots(II.4)$$

m: The mass flow

P_t: Total pressure.

I.5: Effective speed

This is the actual speed measured at the outlet of a nozzle, it is a function of the thrust force e generated by a suitable nozzle and the flow passing through it [29].

$$V_{eff} = F/m \dots\dots\dots(II.5)$$

I.6: The specific impulse

It is a very important entity in the field of propulsion, it is generally used to compare the performance of different propellants, it is expressed in thrust by the product of mass flow and gravitational acceleration

$$I_s = \frac{F}{mg} \dots\dots\dots(II.6)$$

1.7. The total impulse

It is the integral of the thrust during the entire operating time noted by I:

$$I = \int_0^T F dt \dots \dots \dots (II.7)$$

II: DIFFERENT OPERATING MODES OF NOZZLES

Imagine a system consisting of De Laval nozzles. The upstream end of the nozzle is in communication with a tank containing gas that creates a pressure P0, which is assumed to be fixed. Laval divergence creates an almost infinite closed space in which the static pressure Pa can vary.

When the back pressure equals the stop pressure, the liquid comes to a complete rest. The pressure Pa in the downstream reservoir gradually decreases below an assumed constant pressure P0, distinguishing five specific flow situations [25].

II.1: Subsonic flow

The flow through the nozzle is initially subsonic and is characterized by:

- On convergence, velocity increases and pressure decreases to a minimum value that reaches the neck.
- Since the nozzle reduces the speed and increases the pressure to the downstream pressure Pa, the pressure at the throat is minimized or the speed is maximized. Gas evolution is represented by curve (A).

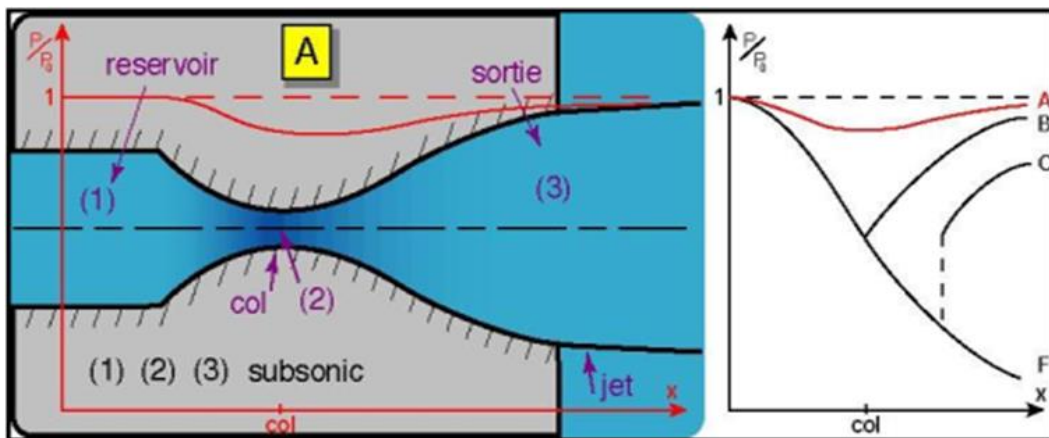


Figure (II.2): Subsonic regime

II.2: Adapted sonic flow

If Pa continues to decrease until there comes a time when the RPM at the neck becomes sonic.

The flow rate is said to be sonically matched.

Let P_{c1} be the downstream pressure for which this phenomenon occurs, throughout the path of the nozzle the regime remains subsonic, with the exception of the neck level where the pressure reaches its minimum value on the other hand the speed reaches its maximum which is its own is in this region. The following figure clearly shows the evolution of the pressure along the nozzle in the regime mentioned above.

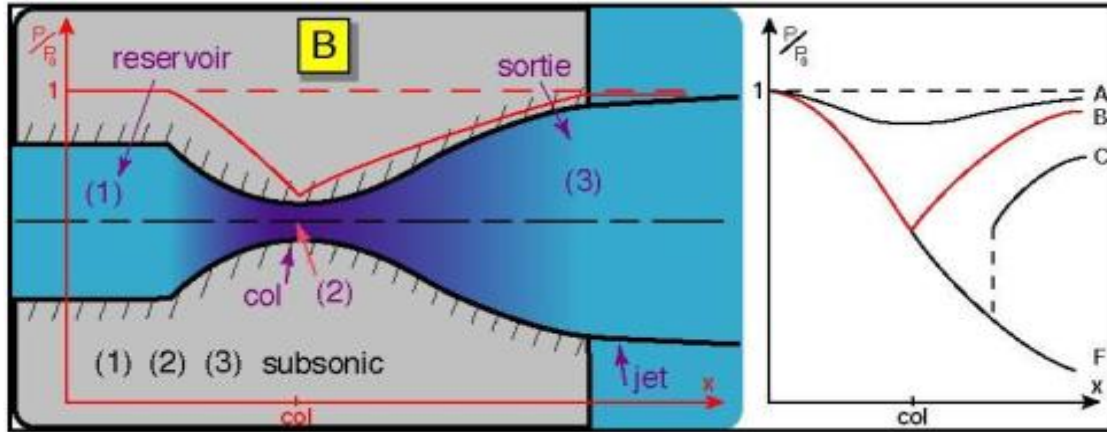
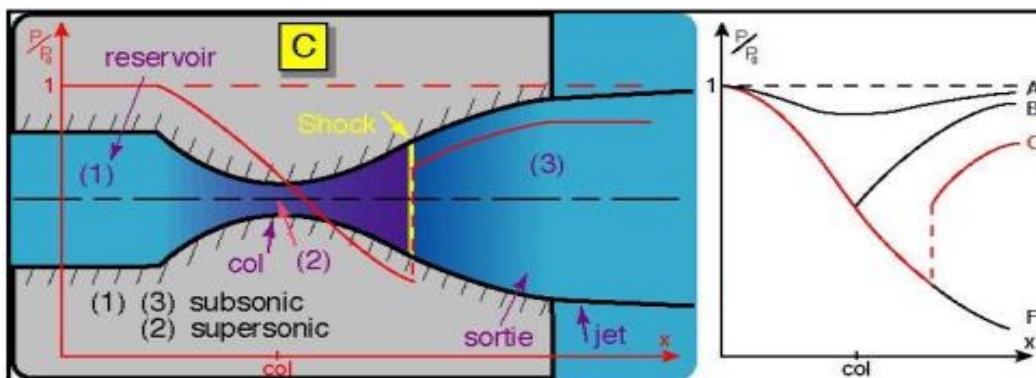


Figure (II.3): Adapted sonic flow

II.3: Unsuitable sonic flow

If P_a is further reduced below P_{c1} , the cervix remains sonic and the cervix is critical. In the divergent part, a shock wave occurs, which produces a sudden increase in pressure and a change in speed state from supersonic to subsonic. The flow is said to be incompatible with sound waves. The evolution of the pressure ratio is represented by the curve (C) in the figure below.

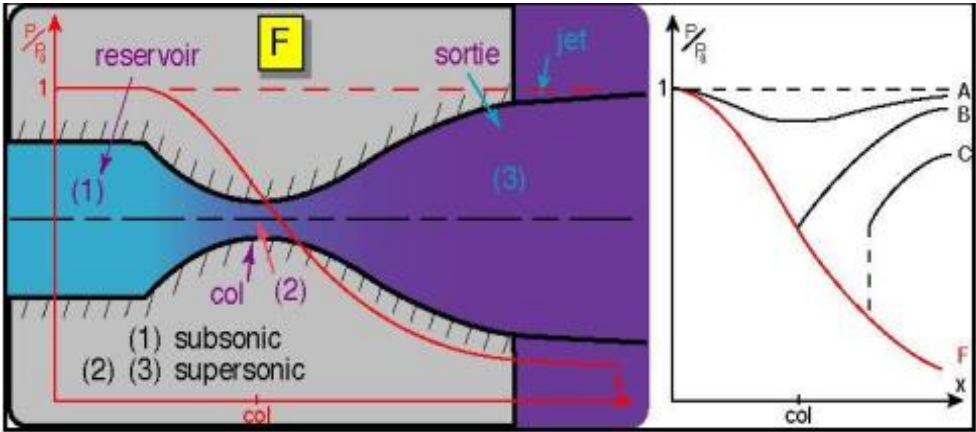


Figure(II.4) : Unsuitable sonic flow

II.4: Adapted supersonic flow

If P_a continues to decrease, there is a point where the flow through the entire nozzle is completely supersonic. The shock wave phenomenon disappears and there is no longer any external compression, the nozzle adapts perfectly, and the evolution of the pressure ratio is

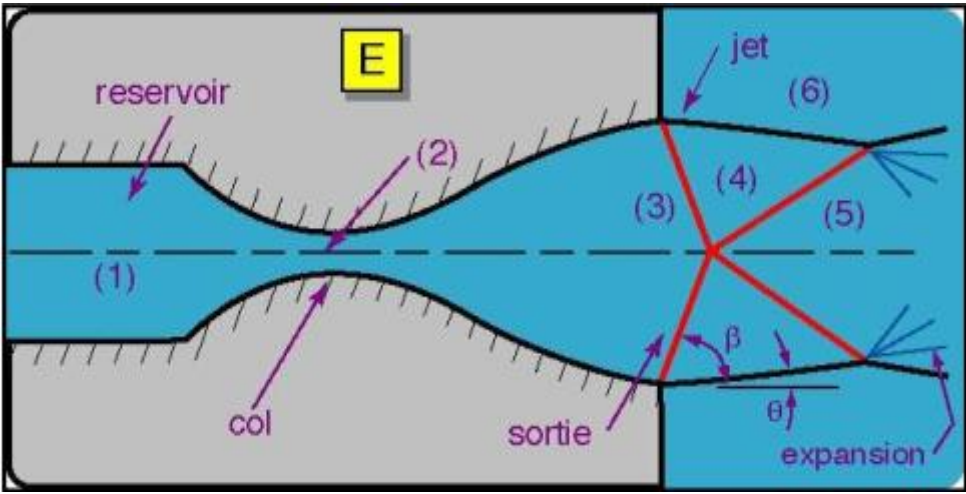
represented by the curve (F) in the figure below. Let P_{ac3} be the downstream pressure at which this phenomenon occurs.



Figure(II.5): Adapted supersonic speed

II.5: Unsuitable supersonic flow

When the pressure P_a is less than P_{ac3} , the flow is said to be non-adaptive supersonic, the flow inside the Laval nozzle does not change at all, the change between the nozzle and the downstream pressure must occur outside of the nozzle, by a series of oblique expansion waves.



Figure(II.6) Régime supersonique non adapté

Chapter III :

Simulation of supersonic flows
in nozzles

I:INTRODUCTION

Numerical simulation of fluid dynamics, commonly known as CFD (Computational Fluid Dynamics), has become a favored tool for scientific and technological research. Its purpose is to computationally reproduce the behavior of a system described by a model, often consisting of partial differential equations. These equations correspond to mathematical transformations of scientific laws. Numerical simulations therefore enhance the mathematical investigation (analysis) of these equations and their numerical resolution. The inner flow is characterized by no boundary conditions at infinity, which is not the case for the outer flow. Therefore, wall effects are evident in all directions, except perhaps at the fluid inlet and outlet. Such flows are especially common in aircraft and rocket propulsion systems. Characterization and identification of internal flows in supersonic nozzles represent a very interesting case study given the complexity of modelling internal flows transitioning from subsonic to supersonic, and thus the significant compressibility effects. Flow structures are diverse (impingement, boundary layer separation, recirculation zones). These serious phenomena make numerical simulations difficult. Experience fuel simulation. Conversely, exploring many possible solutions through simulation helps extend knowledge by observing or predicting unexpected behaviour. Fluid flow, whether internal or external, in the laminar or turbulent regime, is described by a system of partial differential equations (PDEs). Therefore, all physical phenomena are subject to this system, which consists of the following equations:

Continuity, momentum, and energy relationships to be solved to know the properties of thermal and flow fields.

The discretization phase, the phase of the numerical approach consistent with the choice of discretization method for the chosen mathematical model, consists of two phases:

- Space Discretization (Mesh) ▪ Equation Discretization Space discretization consists of setting up a mesh that replaces the continuous space with a finite number of points where the numerical values of the variables are determined. Once the mesh is defined, the equation can be discretized, converting the equation from differential or integral form into a discrete algebraic equation containing the values of the unknowns associated with each point of the mesh. To implement the digital scheme, do the following:

- Choosing a method to discretize the equations

In this step of analyzing the chosen numerical algorithm, we analyze the quality of the chart in terms of stability and convergence. One of the tools used, ANSYS 19, is a computer-aided design (CAD) tool that allows the design and creation of geometry in 3D/2D and applies simulation. This allows you to build surfaces and volumes from a set of points that define the underlying geometry. Once the geometry is created, it can be exported in various formats to mesh generators and solvers for analysis and simulation. ANSYS 19 is mechanical engineering software that works with many different types of software used in many different areas, including:

Vibration, Fluid Mechanics, Aerodynamics, Heat Transfer, Mechanics. In our study, two ANSYS 19 component systems are used to perform air heat calculations. GEOMETRY, ICEM CFD and FLUENT analysis systems. FLUENT is a solver that uses a 2D or 3D unstructured mesh (using the finite volume method). These networks are:

Triangular meshes (tetrahedral in 3D) or rectangular in unstructured form for simulating all compressible or incompressible flows with complex physics such as turbulence, heat transfer, chemical reactions, and multiphase flows Use one of the structured meshes interpreted as (hexahedral). . A 2D or 3D analysis demonstrates FLUENT's ability to simulate flow characteristics around a supersonic nozzle. This problem is solved with Euler's equations. ANSYS-Fluent has been described in several previous studies

ANSYS, Inc. is a software maker specializing in numerical simulation. The company is headquartered in Canonsburg, Pennsylvania, USA. ANSYS develops, drives and supports simulation software that can be used to predict the behaviour of products in their environment. Its main product is software that implements the finite element method to solve previously discretized models. The company has numerous subsidiaries around the world, especially in Europe and Asia⁴.

II: ANSYS CFX AND FLUENT:

Fluid mechanical simulations can be performed using these two software programs. These are named after the companies that developed them, respectively in February 2003 and He was acquired by ANSYS. NC in February 2006⁵. Fluent is a solver that:

A mesh generator is not included (mesh must be created using mesh software such as Gambit, also published by ANSYS). Fluent is a solver widely used in industry and R&D worldwide. It is often considered a reference in the field of fluid modelling. The model is configured via a graphical user interface. It has a scripting interface for automating the calculation process. One of the advantages of this general-purpose simulation software is that it has a relatively large number of models capable of handling various aspects of fluid dynamics.

Two-phase flow (miscible, immiscible, cavitation, solidification), turbulence (LES, KE, Kw, SA, Reynolds stress, etc.), combustion (premixed and non-premixed), particle transport, microporous media Flows, mobile networks especially come with dynamic capabilities due to mesh reconstruction. You can change the temporal and spatial numerical schemes to improve convergence. Fluent is parallelized and can use multiprocessor systems both within a single machine and in networks (clusters, dual-core, multi-CPU platforms).

FLUENT is a flow calculation software (used for modeling fluid flow and heat transfer). It is written in C and takes full advantage of that language's capabilities. Additionally, an architecture is used that allows multiple processes to run simultaneously on the same workstation or multiple workstations for more efficient execution. This computer code uses the finite volume method as the discretization process. This method solves the integral equations governing flow, such as conservation of mass, momentum, and energy. To do this, FLUENT is programmed to perform the following steps.

- Use mesh to divide the domain into separate control volumes.

- Integrate differential equations for a single control volume to create algebraic equations for variables such as velocity, pressure.
- Linearization of discretized equations and solution of the resulting system of linear algebraic equations. Like any other CFD software, Fluent consists of three parts.

A. Preprocessor/Mesher:

This module allows you to prepare the geometrical configuration of the problem under investigation and mesh it in a very user-friendly yet simple way. We used ICEM CFDs in our work. One of the advantages of this software is its simplicity and robustness in realizing the most complex geometries. Depending on the geometry, ICEM CFD uses a monoblock or multiblock structure for the mesh and allows the generation of two mesh types including tetrahedral and hexahedral meshes. For each configuration (geometry – mesh) a data file (*.msh) must be exported to FLUENT.

B. Solver:

It is possible to numerically define the operating conditions (pressure, ambient temperature, gravity) under which the simulation will be performed and define the boundary conditions (it is also possible to return to already defined and created boundary condition types). Perform numerical solutions of equations of motion (continuity, momentum, heat equations).

C. Processor Station:

Visualization of domain geometries and meshes is possible, but in particular FLUENT allows display of velocity, pressure and temperature fields computed on a line or on a line through the DISPLAY menu, so the display of the obtained results is easier. It will be possible. Part of a field or across an entire field of study. You can also draw curves or profiles of specific variables on predefined lines in FLUENT and export numerical results in a variety of available file formats.

III: FLUID MECHANICS EQUATIONS

Fluid flows in convergent-divergent nozzles are regulated by instantaneous Navier-Stokes equations. These equations express the conservation of mass, momentum and total energy of a real fluid in a control volume taken arbitrarily in the flow domain.

III.1/Conservation of mass equation

$$\frac{\partial \rho}{\partial t} + \frac{\partial}{\partial X_j} (\rho u_j) \dots \dots \dots \text{(III. 1)}$$

Where ρ : is the density of the fluid;
 u_j : the "j" component of the velocity vector

III.2: Conservation of momentum equation

$$\frac{\partial}{\partial t} (\rho u_i) + \frac{\partial}{\partial X_j} (\rho u_i u_j) = \frac{\partial}{\partial X_j} (-P \delta_{ij} + \tau_{ij}) \dots \dots \dots \text{(III. 2)}$$

Where P : is the static pressure.
 δ_{ij} : the Kronecker tensor.
 τ_{ij} : the viscous stress tensor.

III.3: Energy conservation equation

$$\frac{\partial}{\partial t} (\rho E) + \frac{\partial}{\partial X_j} [u_j [(\rho E + P)]] = -\frac{\partial q_j}{\partial x_j} + \frac{\partial}{\partial x_j} (u_i \tau_{ij}) \dots \dots \dots \text{(III. 3)}$$

Where q_j is the heat flux in the j direction, E is the intern energy per unit mass, which is expressed by the following relationship:

$$E = e + \frac{1}{2} u_k u_k \dots \dots \dots \text{(III. 4)}$$

We must also add the equation of state of ideal gases:

$$P = \rho \cdot r \cdot T \quad ; \quad C_p - C_v = r \quad ; \quad \gamma = \frac{c_p}{c_v} \dots \dots \dots \text{(III. 5)}$$

γ being the ideal gas constant.

A. Stress tensor: For an assumed Newtonian fluid, the viscous stress tensor takes the following form:

$$\tau_{ij} = \mu \left(\frac{\partial u_i}{\partial x_j} + \frac{\partial u_j}{\partial x_i} \right) + \lambda \delta_{ij} \left(\frac{\partial u_j}{\partial x_j} \right) \dots \dots \dots \text{(III. 6)}$$

Where μ and λ are related by the Stokes hypothesis: $3\lambda + 2\mu = 0$
The heat flux per unit area q_j as a function of temperature is written as follows:

$$q_j = -k \frac{\partial T}{\partial X_j} \dots \dots \dots \text{(II.7)}$$

k : is the thermal conductivity which is expressed as a function of the dynamic viscosity by the Prandtl number Pr:

$$Pr = \frac{u c_p}{k} = \gamma \frac{u c_v}{k} \dots \dots \dots \text{(III. 8)}$$

Assuming the fluid is calorifically perfect the internal energy $e = C_v \cdot T$ and the enthalpy $h = C_p \cdot T$, the heat flux can be written:

$$q_j = -K \frac{\partial T}{\partial x_j} = -\frac{\mu}{Pr} \frac{\partial h}{\partial x_j} \dots \dots \dots (II.9)$$

With regard to the dynamic viscosity, this one is given, for the range of studied temperature, by the law of Sutherland (used by FLUENT) following:

$$\mu = \mu_0 \sqrt{\frac{T}{T_0} \left(\frac{1+T/T_0}{1+S/T} \right)} \dots \dots \dots (III. 10)$$

Or :

$\mu_0 = 1.78938 \cdot 10^{-5} \text{kg.m}^{-1} \cdot \text{S}^{-1}$ is the viscosity of the fluid at the reference temperature;

$T_0 = 288\text{K}$;

S: is a fixed constant for air at 110 K.

IV: MEAN EQUATION OF MOTION

IV.1/ Must be average.

The turbulent nature of a flow manifests itself as a fluctuating or chaotic behavior in the flow characteristics. Such fluctuations occur when the Reynolds number of the flow is large. The temporal and spatial scales of this flow are small and are difficult to decompose directly from the Navier-Stokes equations, given the importance of the networks to be implemented.

Navier-Stokes equations still describe the motion of liquids, but directly analyzing liquids requires a lot of computation time and memory. For example, if the flow in the pipe is restricted and the Reynolds number is 104, then 109 points are required. You should limit the amount of information you process, for example calculating only the intermediate fields. We then treat the state variable as a random function of time and space and decompose it into an average computational part and a fluctuating modeling part. This method is called Reynolds decomposition.

Applying this decomposition to the balance equation above gives an equation for the behavior of the fluid in turbulent flow. Nonlinearities in the Navier-Stokes equations introduce new terms, so-called correlations, that need to be modeled.

IV.2: Reynolds equation

Let us now see how the aforementioned averaging principle is taken into account in the Navier-Stokes equations. We briefly describe how to obtain new equations from the instantaneous equations and clarify the closure problem.

IV.3: System Averaging

The goal is to find a form of the mean system that is as close as possible to the original form of the equation. To find the average Navier-Stokes equation, use the Reynolds and Fabre average.

Reynolds says:

If 'f' is an arbitrary function, let \bar{f} denote the statistical (or Reynolds') mean of f. For example, for the density and velocity vectors, we denote the Reynolds means of ρ and u by $\bar{\rho}$ and \bar{u} , respectively, and the varying parts of these variables by ρ' et u' . So it looks like this:

$$\rho = \bar{\rho} + \rho' \text{ ou } \bar{\rho}' = 0 \dots \dots \dots \text{(III.11)}$$

$$u = \bar{u} + u' \text{ ou } \bar{u}' = 0 \dots \dots \dots \text{(III.12)}$$

In the ρ density, it becomes the u velocity component.

Using only the Reynolds average makes some terms difficult to use in the compressible case. In fact, the same composition was applied to the product $\rho \cdot u$ gives:

$$\rho u = \bar{\rho} \bar{u} + \bar{\rho} u' + \rho' \bar{u} + \rho' u' \dots \dots \dots \text{(III.13)}$$

Such :

$$(\rho u)' = \bar{\rho} u' + \rho' \bar{u} \dots \dots \dots \text{(III.14)}$$

Applying the Reynolds averaging to the conservation of mass equation gives:

$$\frac{\partial \bar{\rho}}{\partial t} + \nabla \cdot (\bar{\rho} \bar{u}) + \nabla \cdot (\bar{\rho} u') = 0 \dots \dots \dots \text{(III.15)}$$

This step introduces a new modeled term $\bar{\rho} u'$ into the equation of continuity. Therefore, the closure of the simplest system of mean equations depends at least on knowledge of this relationship. To circumvent this difficulty, it is necessary to use Fabre averaging in the mathematical modeling of compressible turbulence [30].

The B. Fabre family thinks:

If X is a quantity, denote the Fabre mean of X by \bar{X} and the variation of X with respect to the Fabre mean by $\tilde{X} = X - \bar{X}$. Additionally, \tilde{X} is determined from the Reynolds mean.

$$\tilde{x} = \frac{\rho' x}{\rho} \dots \dots \dots \text{(III.16)}$$

In the following we use the Reynolds mean for the density ρ and the pressure field p , and the Fabre mean for the other variables [30].

Finally, the mean equation of motion is:

$$\frac{\partial}{\partial t} \bar{\rho} + \frac{\partial}{\partial x_j} \bar{\rho} \bar{U}_j = 0 \dots \dots \dots \text{(III.17)}$$

$$\frac{\partial}{\partial t} \bar{\rho} \bar{U}_j + \frac{\partial}{\partial x_j} (\bar{\rho} \bar{U}_t \bar{U}_j + \bar{\rho} u_t' u_j') + \bar{p} \delta_{ij} = \frac{\partial}{\partial x_j} \bar{\sigma}_{ij} \dots \dots \dots \text{(III.18)}$$

$$\frac{\partial}{\partial t} \bar{\rho} \tilde{E}_t + \frac{\partial}{\partial x_j} \left[\bar{U}_j (\bar{\rho} \tilde{E}_T + \bar{P}) + \bar{\rho} u_j' h' \right] + \frac{1}{2} \bar{\rho} u_i' u_k' \tilde{U}_k + \frac{1}{2} \bar{\rho} u_j' u_k' \tilde{U}_k = \bar{\sigma}_{ij} \bar{U}_i - \bar{q}_j \dots \dots \dots \text{(III.19)}$$

Fabre's mean clearly shows that it is possible to hide (obscure) connections by accounting for density variations. This feature also allows Fabre formalism to maintain a conservative form of the instantaneous equation.

The definition of total energy changes as follows:

$$E_t = \tilde{e} + \frac{1}{2} \widetilde{U_K U_K} + \frac{1}{2} \widetilde{u_k u_k} \dots \dots \dots (III. 20)$$

where "E" is the total energy.

unit of mass. At the same time, we also obtain the formulation of the equation of state.

$$\bar{P} = \bar{\rho} \tilde{T} = \bar{\rho} (\gamma - 1) \tilde{e} \dots \dots \dots (III. 21)$$

V: DIFFERENT TYPES OF RIVERS

, we briefly describe some types of flows qualitatively.

V.1: Incompressible and Compressible Flows

A liquid is said to be incompressible if its specific mass changes slightly with pressure or temperature. The relative specific mass change of water is therefore $\Delta\rho/\rho = 5 \times 10^{-4}$ for a temperature change $\Delta T = 1\text{K}$ and $\Delta\rho/\rho = 2 \times 10^{-4}$ for a pressure change $\Delta p = 1\text{ bar}$. Therefore, we can often treat water as an incompressible liquid and use the density $\rho = \rho_0 = \text{constant}$ in the equations of motion. For gas:

Gases are generally treated as compressible liquids. However, at low flow velocities (small Mach numbers before $M \ll 1$), we find that the density change is small in magnitude as the square of the Mach number [31].

$$(\Delta\rho)/\rho = M^2 \quad M \ll 1 \dots \dots \dots (III. 22)$$

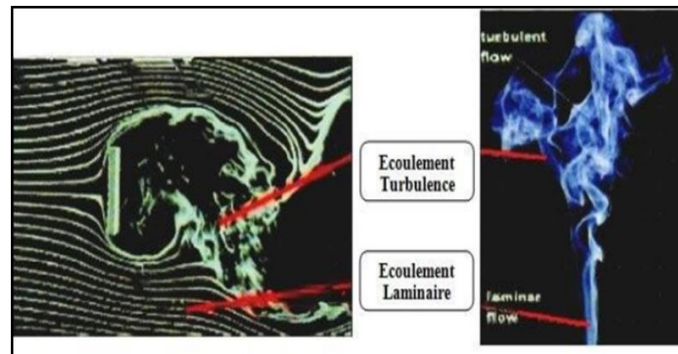
V.2: Laminar and turbulent flow

Turbulence can be characterized by the random placement (or variation) of velocity vectors at each point. In other words, each component $u(M, t)$, $v(M, t)$, $w(M, t)$ of $V(M, t)$ has a distribution law (in the probabilistic sense) as a function of space and time follow. The flow conditions must be turbulent. Turbulence may be time-dependent, but in a more "regular" way, it may have an average component \bar{a} (eg, the movement of the earth from west to east). Fluctuations occur around this average ratio, thus changing the speed.

In laminar flow, a liquid travels in parallel "layers", each with its own velocity. There is order in the control of velocity in moving liquids. A velocity vector maintains a stable direction over time. This flow condition is called laminar flow.

When the laminar motion of a fluid changes to turbulence, it loses its ordered and stable properties. We say that there is a transition from a laminar to a turbulent state, or more simply a turbulent-laminar transition.

The difference between turbulent and laminar regimes can be represented by a curve giving velocity as a function of time at a fixed-point M.



Figure(III. 1) : Laminar flow and turbulent flow

V.3. Steady flow and transient flow

A flow is said to be stationary if, at any point M in Ω , all the variables describing the motion are independent of time. Therefore, the steady flow pressure P, velocity v, density ρ , and energy e are time-independent quantities.

$$\vec{V}(M, t) = \vec{V}(M) \quad \forall M \in \Omega \dots \dots \dots (III. 23)$$

All wave propagation phenomena in liquids fall into this category (waves on the surface of liquids, emission of sound waves from turbulent free streams, etc.). Air currents are also inherently unstable.

Turbulence is also inherently unstable. However, turbulence is said to be unstable if the mean variables are independent of time and the quadratic correlations formed from these variables are transition-invariant [31].

V.4. Irrational flow

We say that the flow in a region D is irrational at a particular time t if the rotation of the velocity $\vec{V}(M, t)$ is zero at each point M in D. It is written symbolically [31]:

$$(\text{Red}) \quad \text{rot} \vec{V}(M, t) = \nabla \times \vec{V}(M, t) \dots \dots \dots (III. 24)$$

For example, it is written in Cartesian coordinates.

$$\text{rot} \vec{V}(M, t) \left[\frac{\partial w(M, t)}{\partial y} - \frac{\partial v(M, t)}{\partial z} \right] \vec{X} + \left[\frac{\partial u(M, t)}{\partial z} - \frac{\partial w(M, t)}{\partial x} \right] \vec{y} + \left[\frac{\partial v(M, t)}{\partial x} - \frac{\partial u(M, t)}{\partial y} \right] \vec{Z}..$$

VI. TURBULENCE PATTERN

Turbulence is characterized by a fluctuating velocity field. These fluctuations perturb transport quantities such as energy and species concentrations. These variations can be small and frequent, and are computationally very difficult to simulate directly in technical practice calculations.

Alternatively, the direct (exact) governing equations can be replaced by time-averaged equations reduced to a smaller structure to obtain a set of modified equations that are easy to solve [32]. 5.1. Sparto Almaraz model

The Spalart-Allmaras model is a simple one-equation formulation. This model is specifically aimed at aerospace applications and gives satisfactory results for boundary layer calculations subjected to very strong pressure gradients. Other applications such as turbomachinery are also growing in popularity.

In its original formulation, the Spalart-Allmaras model is a low Reynolds number turbulence model that requires a complete solution of the boundary layer equations.

However, some of his CFD codes combine this model with wall functions if the mesh resolution is not fine enough. Moreover, this model is less sensitive to numerical errors than the $k-\varepsilon$ and $k-\omega$ models [32].

VI.1: The $k-\varepsilon$ model:

The most common turbulence models are the so-called two-equation models, including the $k-\varepsilon$ model. It is commonly used in many engineering calculations. It is based on the formulation proposed by Launder and Spalding.

Its robustness, economy, and accuracy in predicting a wide range of turbulence problems explain its popularity in industrial flow simulation and heat transfer problems. The $k-\varepsilon$ model is a semi-empirical model and the equations used are based on phenomenological and empirical considerations.

Compared to the original formulation, the model has been refined to better fit the specific flow case. Thus, we find the variant $k-\varepsilon - \text{RNG}$ (renormalization group) and the $k-\varepsilon$ correction value [32].

VI.2: Standard $k-\omega$ model and $k-\omega\text{-SST}$ model:

The $k-\omega$ model is based on the Wilcox equation modified to account for effects related to low Reynolds and compressibility. Two variants of the $k-\omega$ model, Standard and SST, are semi-empirical models that have the same mathematical form as the transport equations for k and ω . The $k-\omega\text{-SST}$ model is based on the formulation proposed by Menter [32].

VI.3: Reynolds stress model RSM:

This model has been further refined. The assumption of turbulent viscosity isotropy is circumvented to solve the equation for the six Reynolds stress components and ϵ . Therefore, the model is often very numerically heavy and difficult to converge. There are many variations on this model, especially regarding the method used to model the correlation between pressure fluctuations and strain. This model is recommended for highly turbulent flows such as cyclones and injectors in combustion boilers [32].

VI.4: Large Eddy Simulation (LES) :

The LES approach resolves all turbulent scales except the diffuse scale modeled. Therefore, you should use a very fine mesh and choose a transient solution when solving the equations. After a sufficiently long computation time, the solution can recover all turbulence scales. This model works very well when the flow is not dominated by the presence of walls.

TABLEAU III.1 advantages and disadvantages of turbulence models

Models	Advantages	disadvantages
Spart-Almaras	Economic (1 Eque). Good for moderately complex flows.	Not widely tested.
STD k-ϵ	Robust, economical and relatively precise.	Poor results for complex flows.
RNG k-ϵ	Good for moderately complex flows	Limited by the assumption of isotropic turbulent viscosity.
Réalisable k-ϵ	Offers the same benefits as RNG.	Limited by the assumption of isotropic turbulent viscosity.
Reynolds Stress Model (RSM)	The most physically complete model.	Requires more CPU time. The momentum and turbulence equations are related.
SST et Standard k-ω	The most recommended model for turbomachinery related problems.	Requires higher mesh resolution at boundaries.

VII: TRADITIONAL NUMERICAL METHODS IN CFD

Several methods are used in CFD to solve the hydrodynamic equations. Discretization of PDEs can be performed using three techniques:

Finite difference method, finite volume method, finite element method [33].

VII.1: Finite difference method:

The finite difference method was first formulated by Euler in 1978 [34]. It is one of the most widely used numerical methods for finding approximate solutions to systems of partial differential equations. It is very easy to implement and allows very accurate reconstructions [34].

The finite difference method implementation is formulated as follows.

Put the equation in differential form.

Create a mesh that covers the computational domain.

Discretize the differential equation and fit it on a mesh. So we get the Taylor expansion of the variable $U(x)$.

$$U_{(i-1)}=U_i-(\partial U/\partial X)_i \Delta X+ ((\partial^2 U)/(\partial X^2))_i (\Delta X^2)/2+\dots\dots\dots(III. 24)$$

$$U_{(i+1)}=U_i+(\partial U/\partial X)_i \Delta X+ ((\partial^2 U)/(\partial X^2))_i (\Delta X^2)/2+\dots\dots\dots(III. 25)$$

Subtracting the previous two expressions gives an approximate first-order expression.

$$(\partial U/\partial X)_I=U_{(i+1)}/2\Delta X+0(\Delta X)\dots\dots\dots(III. 26)$$

Adding them together gives a quadratic approximation.

$$((\partial^2 U)/(\partial X^2))_I=(U_{(i+1)}-U_i+U_{(i-1)})/(\Delta X^2)+0(\Delta X^2)\dots\dots\dots(III. 27)$$

The finite-difference method has the advantage that higher-order schemes can be easily formulated. However, its weakness lies in the fact that it can only be applied to structured networks [35].

VII.2: Finite element method

The process first divides the domain boundary into line segments. Next, we formulate the problem using marginal integrals only. The unknown variables can be calculated at specific points of the boundary, the so-called Zienkiewicz and Taylor nodes [34]. Nodes are typically midpoints or endpoints of discrete boundary segments [36].

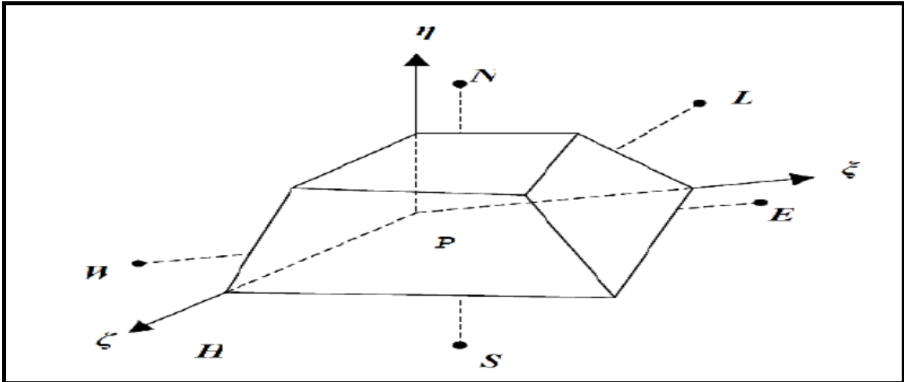
VII.3/ Finite volume method

In the finite volume method, the domain is split into a set of control volumes that overlap with the computational domain. Conservation laws are applied to each volume or control to determine various variables relevant to the problem at points (or nodes) that do not necessarily correspond to points on the mesh. This method results in a very large selection of control organs and nodes (central cells, cell vertices, node vertices). The computationally relevant mesh can be structured or unstructured, similar to the finite element method, giving the method great flexibility. One of the main advantages of this method is that the spatial discretization is done directly in the physical domain. Therefore, no conversion takes place between different coordinate systems.

"Finite volume" type formulations are based on a discretization of conservation laws, and these laws are, of course, satisfied by numerical schemes for control volumes. This property is important when dealing with shocks (or other kinds of discontinuities) as it ensures that the Rankine-Hugonio relation is satisfied .

This method is used in major existing commercial laws.

Phonics, Fluent, Flow 3D, Star CD,



Figure(III. 2) : Control volume in a three-dimensional configuration

VIII: DISCRETIZATION OF COMPUTATIONAL DOMAIN

Network operations involve discretization of the computational domain. Mesh generation is an important part of his CFD, as the quality of the mesh has a large impact on the convergence of the flow solver and the accuracy of the solution obtained on the mesh.

VIII.1: Network

Mesh generation is an important part of creating a CFD simulation. This is a necessary first step, as without a suitable mesh no numerical simulation can be performed. This logic consists of modeling a physical problem through a system of equations and solving it in a computational domain representing a particular geometry.

Several methods have been developed to help users of numerical tools generate meshes in the best possible way. Choosing the type of fabric is often a problem.

- The first choice is between structured and unstructured meshes based on solver properties and geometric complexity.

- The second option is to select the item type. Once the mesh is generated, the solver (e.g. fluent) evaluates area and volume based on grid point coordinates and element geometry [29].

VIII.2: mesh concept

a- nodes and elements:

Numerical modeling is based on reformulating the conservation equations for elementary or discrete volumes Ω called elements or cells. These elements contain the nodes of the discretization, the decomposition points of the discrete equations. Depending on the discretization method used, these can be placed at the corner points of the element, at the middle of the element, or on the surface. Related elements and nodes form a network [29].

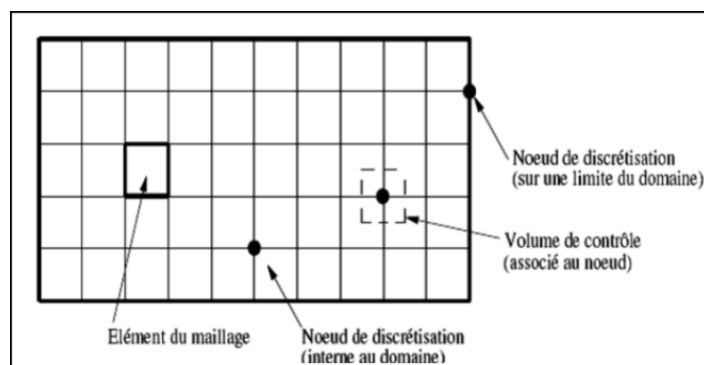


Figure (III. 3) : *Illustration of the concept of the mesh*

VIII.3: CLASSIFICATION OF MESH METHODS

Meshes are classified according to their properties or the method used to create them. In the following, only the main features of this classification are presented [29].

- Networks are characterized according to their properties.
 - A structured set of rules.
 - Adjusted curves.
 - Unstructured.
 - hybrid. - By geometric shape.
 - Depending on the generated method:
 - Hyperfinite interpolation or algebraic methods.
 - Differential equations or conformal transformations.
 - Delaunay triangulation.
 - Advance. - Breakdown per block.
 - Hierarchical division.

VIII.4.1: Structured mesh

Structured meshes can be considered the most natural for flow problems. Since flow is generally aligned with solids, you can think of the grid lines going in the same direction as the streamlines.

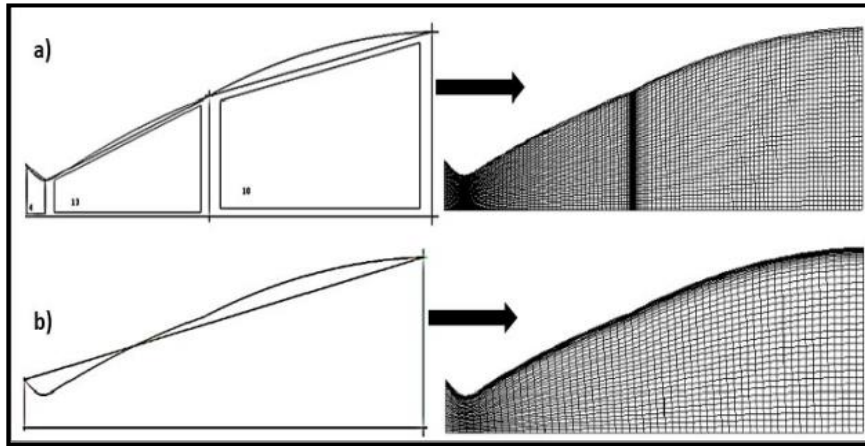
Domains consist of two-dimensional (2D) square or cubic cells, and nodes are identified by pairs of two-dimensional (or three his three-dimensional) numbers that indicate their position in the lattice [29]

VIII.4.2: TECHNIQUES FOR CREATING STRUCTURED MESHES.

a- multi-block method:

A structured multi-block network is generated by manually dividing the domain into blocks of simple form and constructing each block in a structured way. The user can define the number of nodes and their distribution along each edge of the block. Below is a 2D view of a hexagonal polygon mesh inside a double curvature nozzle. Block system on the left, mesh on the right.

Despite the difficulties in fabricating structured grids, this offers undeniable advantages, especially in viscous flows. To solve the boundary layer flow, it is relatively easy to create a square mesh with elongated elements in the direction parallel to the walls. Placing the edge perpendicular to the wall is also easy. This minimizes the error in estimating velocity gradients near walls. Finally, after creating the block, it is relatively easy to change the mesh density by placing the mesh points according to the needs of the solver [29].



*Figure(III. 4) : Structured mesh in a double curved nozzle,
(a multi-block, b mono-block)*

VIII.4.3: UNSTRUCTURED NETWORKS

Triangular meshes are the most common type of unstructured mesh. Triangular meshes can be connected in many ways, so any area can be easily filled with any shape. The connections are so flexible that different techniques can be used to create this kind of mesh [29].

a- Techniques for generating unstructured networks:

The most commonly used techniques are:

- Delaunay.
- move forward.
- Octree method.

VIII.4.4: HYBRID MESH

A mesh generated by mixing different types of elements. In 2D they are triangles or quadrilaterals, and in 3D they are tetrahedrons, prisms, or pyramids.

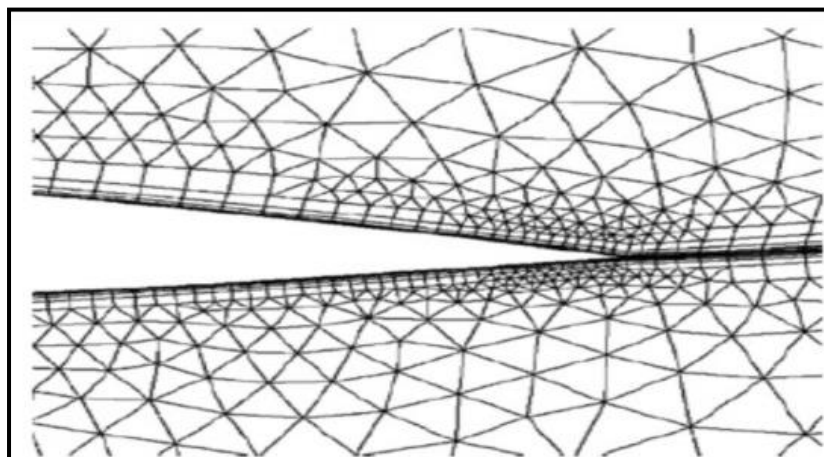


Figure (III. 5) : Hybrid unstructured mesh

IX: COMPARAISON BETWEEN STRUCTED AND UNSTRACTED MESH

TABLEAU III.2 *Structured Mesh and Unstructured Mesh*

	structured mesh	Unstructured mesh
advantages	<p>It is much easier to generate it using multi-block geometry.</p> <ul style="list-style-type: none"> • Economical in number of elements. <p>Has a lower number of meshes compared to an equivalent unstructured mesh.</p> <ul style="list-style-type: none"> • Reduces the risk of numerical errors, because the flow is aligned with the mesh. 	<ul style="list-style-type: none"> • Can be generated on a complex geometry while keeping a good quality of the elements. • The generation algorithms for this type of mesh are highly automated. • Unlike structured meshes, there are no restrictions on the topology of the domain.
disadvantages	<ul style="list-style-type: none"> • Difficult to generate in complex geometries. • Difficult to obtain mesh quality for complex geometries. 	<ul style="list-style-type: none"> • Very greedy in number of meshes compared to the structured mesh. • Generates numerical errors, which can be very large if compared with the structured mesh

X: CONCLUSION

This chapter has described the fluid dynamics equations that govern fluid flow in a converging-diverging nozzle.

The choice of turbulence model depends on the nature of the problem, its quality, and the computational time and effort.

We also discussed the discretization of the computational domain and the generation of the mesh. This is an important factor in CFD, as the quality of the mesh can have a large impact on the convergence of the flow solver and the accuracy of the solution obtained. on the web.

/ LÄŃ'nlē

wəŋ ü[ŋ

INTRODUCTION:

In a supersonic nozzle, side loads refer to the forces exerted on the walls of the nozzle due to the high-speed flow of gases. These side loads can have various causes and implications, which are important to consider in the design and performance optimization of the nozzle.

One major factor contributing to side loads is the aerodynamic forces generated by the supersonic flow of gases. These forces arise from the pressure differential between the inside and outside of the nozzle and the changes in flow direction. The magnitude of these forces depends on the nozzle geometry and the operating conditions.

Another factor that contributes to side loads is the presence of shock waves. In supersonic flow, shock waves form when the flow velocity exceeds the local speed of sound. These shock waves can interact with the walls of the nozzle, leading to additional forces and loads. The intensity and location of the shock waves depend on the design and operating parameters of the nozzle.

Boundary layer effects also play a role in side loads. The boundary layer is a thin layer of slower-moving gas that forms along the walls of the nozzle due to viscosity. The presence of the boundary layer affects the pressure distribution on the walls, which can result in side loads.

Considering structural considerations, the side loads experienced by a supersonic nozzle must be taken into account in its design. The materials used, as well as the shape and reinforcement of the nozzle, should be able to withstand these loads to ensure structural integrity and prevent failure.

To mitigate side loads, engineers employ various techniques. One approach is optimizing the nozzle shape to minimize the generation of aerodynamic forces and shock waves. Additionally, the use of shock-absorbing materials can help attenuate the impact of shock waves on the nozzle walls. Structural reinforcements are also employed to enhance the overall strength and durability of the nozzle.

To analyze and optimize nozzle designs, engineers often utilize computational fluid dynamics (CFD) simulations and wind tunnel testing. These techniques allow for a detailed analysis of the flow behavior and its impact on side loads, enabling engineers to make informed

design decisions to minimize side loads and maximize the efficiency and performance of the supersonic nozzle.

In this study, our focus was to investigate the influence of the central body on the lateral forces and efficiency of the nozzle. By understanding and mitigating side loads, we aim to enhance the overall performance and reliability of supersonic nozzles in various applications.

I: 16-FOOT TRANSONIC TUNNEL (BUILDING 1146)

A detailed experimental study of separated nozzle flows has been conducted at the NASA Langley Research Center 16-Foot Transonic Tunnel Complex. As part of a comprehensive static performance investigation, force, moment and pressure measurements were made and schlieren flow visualization was obtained for a subscale, non-axisymmetric, two-dimensional, convergent-divergent nozzle. For reference, experimental results were compared with theoretical predictions based on one-dimensional gas dynamics and an approximate integral momentum boundary-layer method. Results from this study indicate that over-expanded nozzle flow was dominated by shock-induced boundary-layer separation, which was divided into two distinct flow regimes: three-dimensional separation with partial reattachment and fully detached two-dimensional separation. The test nozzle was observed to go through a marked transition in passing from one regime to the other. In all cases, separation provided a significant increase in static thrust efficiency compared to the ideal prediction. Results suggest that, with controlled separation, the entire overexpanded range of nozzle performance would be within 16% of the peak thrust efficiency. By offering savings in weight and complexity over a conventional mechanical variable geometry exhaust system, a fixed geometry nozzle may be able to cover an entire flight envelope in some applications.

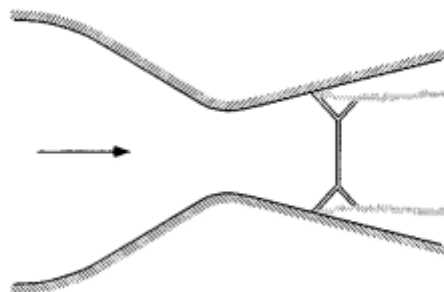


Figure IV.1 Overexpanded CD Nozzle with Separation

Year Built: 1941

Historic Eligibility: National Register Eligible

Important Tests: A-26 Invader; X-1; P-1127; Titan Rocket; F-111 Aardvark; B-58 Hustler; F-14 Tomcat; F-15 Eagle; F-18 Hornet; B-1A Lancer; B-2 Spirit; X-20 Dyna-Soar; Test 191: Apollo Moon Mission Spacecraft; Saturn Rocket; Space Shuttle; C-5M Super Galaxy; Test 420: NASP; X-45; NATF; HIMAT.

Year Demolished: 2011 (tunnel component)

In the late 1930s, the Special Committee on Future Research Facility proposed building at Langley a wind tunnel with a 16-foot-diameter test section that could assess engine and propeller cooling. of large aircraft.

Construction approval was granted in 1939. The new 16-foot High Speed Tunnel (HST) opened in November 1941 and began trial runs on December 5, 1941, just two days before the attack. Japanese attack on Pearl Harbor. After the war, in addition to engine cooling, testing also focused on wing/wing/elevator vibration and bomb/missile aerodynamics. Although the 16-foot HST was never Langley's largest or fastest wind tunnel, it played an important role in the development of post-war tunnel design. In the late 1940s, physicist Ray H. Wright of Langley observed that interference from the walls of a wind tunnel could be minimized by placing slits in the neck of the test section, a concept known as is "split neck" or "slit wall". trial section.

While testing this new design at 16 ft HST, Langley engineers found it allowed supersonic speeds (up to and in excess of the speed of sound, Mach 1, approximately 761 mph at water level. sea). Small circular "parasitic" test sections operate at speeds up to Mach 1.6 by drawing outside air through a long diffuser into the low-pressure test section of the 16-foot HST. The award-winning slotted test piece Collier Trophy was first shown to work in one of these in 1947. Refitted with new grooved test piece throat and increased power 60,000 horsepower, the facility was renamed the 16-foot Transonic Tunnel. (TT) December 1950.

Work on the slotted test section in 16ft HST was instrumental in helping John Stack (Head of Department) and his associates the Collier Trophy for the design, development and practical application of the crosstalk wind tunnel throat.

II: TEST NOZZLE

Experimental testing was conducted in the model preparation area of the NASA Langley 16-Foot Transonic Tunnel Complex. This facility is normally used for the build-up and calibration of wind tunnel models but can also be used for nozzle testing at static conditions.

Models are mounted on a sting-strut support system in a 10x29 foot ambient test chamber, and supplied with a regulated continuous flow of clean, dry air. A control room adjacent to the test chamber offers access through a soundproof door and observation window. A complete description of this test facility is provided in reference 5

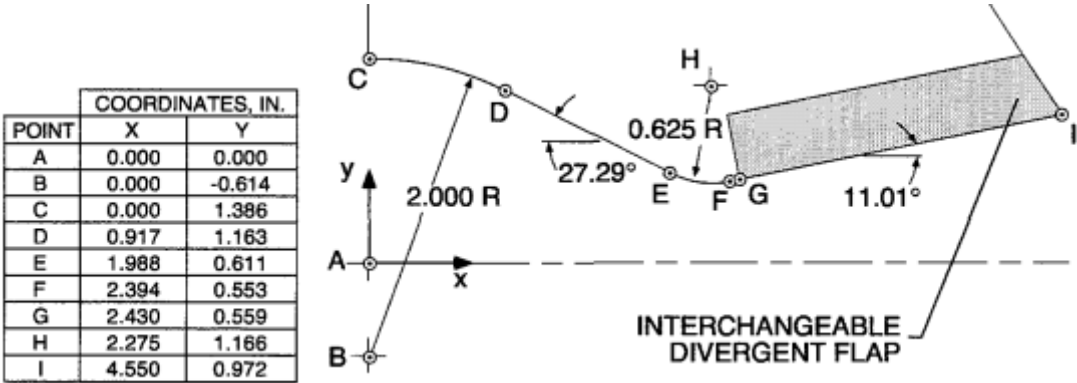


Figure IV.2 Nozzle Flap Geometry

The test nozzle used in this investigation was a subscale, non-axisymmetric, two-dimensional convergent divergent (2D-CD) nozzle with a nominal throat area $A_t=4.317$ in², an expansion ratio $A_e/A_t=1.797$, and a constant width of 3.990 inches. Based on ID Theory, the nozzle has a design NPR of 8.78, an exit Mach number of 2.07, and a design throat Reynolds number of 3.2×10^6 for $p_a=14.85$ psi. The nozzle was equipped with interchangeable divergent flaps in order to function as a testbed for various shock - boundary layer interaction control concepts and had full length optical quality glass sidewalls to allow for internal flow visualization and flow diagnostics. Geometric details of the nozzle are shown in figure IV.2, and a photo of the nozzle is given in figure IV.3

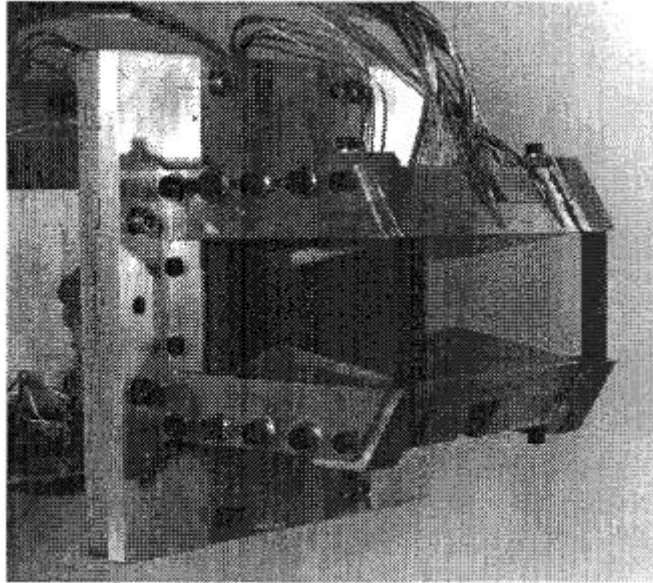


Figure IV.3 *Test Nozzle*

II-1: Flow visualization

A focusing schlieren system was used to visualize internal nozzle flows in this study. Based on criterion developed by Weinstein⁹, the system had a 133 mm diameter field of view, a sensitivity of 17 arcsec, a resolution of 0.25 mm, a depth of sharp focus of 4.6 mm, and a depth of unsharp focus of 36 mm. The light source for the schlieren system was a xenon strobe flash tube, driven at a 30 Hz rate with pulses of 0.6 p.sec duration and 0.05 watt-sec power. The system was focused on the test nozzle centerline plane and configured for sensitivity to streamwise density gradients. A 720x480 pixel resolution video camera and 70 mm Hasselblad still camera recorded results.

II-2: Experimental results

In this section, experimental results will be presented in terms of internal flow features (static pressure measurements and schlieren flow visualization) and thrust performance. Because the test nozzle had glass sidewalls that flexed slightly under pressurization, it was not possible to accurately measure discharge coefficient and these data are not presented. Internal Flow Normalized experimental centerline static pressures (p/p_0) are presented in figure 8, plotted against nondimensional streamwise location. Results are representative of classic CD nozzle flow¹⁶. For the first data points at NPRs 1.25 and 1.4, pressure data indicate choked, internally overexpanded flow with a weak shock near the

geometric throat. Flow downstream of the shock appears to recover to ambient pressure ($p/p_0j=1/NPR$) in a smooth continuous fashion. Focusing schlieren flow visualization obtained at $NPR=1.4$ is presented in figure 9, and shows a weak, almost normal shock downstream of the nozzle throat with little or no lambda foot structure evident. This shock - boundary layer interaction is characteristic of a weak shock ($Mi=1.2$, estimated from p/p_0j) and a thin boundary layer. __ Poj 1.0

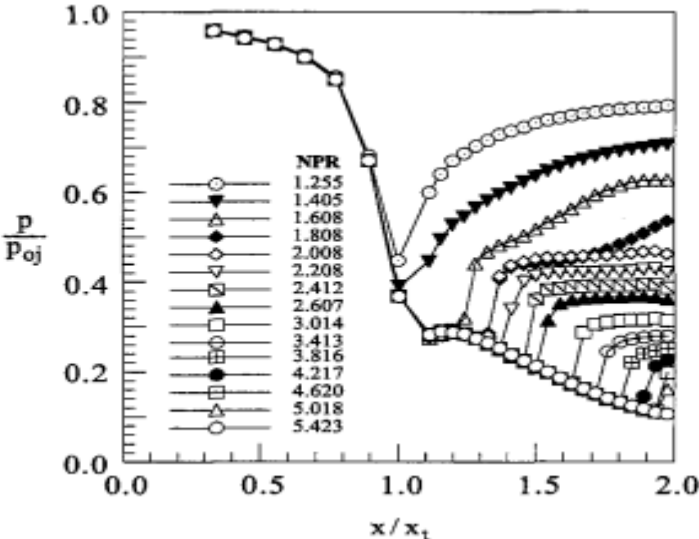


Figure IV.4 Experimental Centerline Pressure Data

In order to improve these results we did a simulation using ANSYS 19

III: NUMERICAL SIMULATION

Simulation software has revolutionized the way we study and analyze designs, providing highly accurate calculations and taking into account numerous parameters. One widely used tool in both research and industry is the Fluent code. This powerful software enables numerical simulations of viscous flow, making it an invaluable resource in our study.

In the numerical analysis of flow through a nozzle, Fluent solves the Navier-Stokes equations using a Reynolds Averaged Navier-Stokes (RANS) approach. This approach provides a reliable and efficient method for modeling turbulent flows. Turbulence plays a significant role in nozzle flows, and to accurately capture its effects, various turbulence models can be employed.

One commonly used turbulence model is the Reynolds-averaged Navier-Stokes (RANS) model. It averages the flow variables over time, resulting in the estimation of Reynolds stresses that appear in the Navier-Stokes equations. These models, such as the k-epsilon model or the SST (Shear Stress Transport) model, allow us to capture the complexities of turbulent flow and its impact on the behavior of the nozzle.

By employing Fluent and appropriate turbulence models, we can conduct a comprehensive numerical analysis of the flow through the nozzle. This analysis provides insights into critical parameters such as velocity distribution, pressure distribution, and the occurrence of phenomena like shock waves and separation. It allows us to understand the flow characteristics, optimize the design, and make informed decisions to enhance the performance of the nozzle.

The use of simulation software like Fluent not only saves time and resources by eliminating the need for extensive experimental testing but also enables us to explore a wide range of design possibilities and operating conditions. It provides a reliable and cost-effective means to assess the performance and reliability of nozzle designs before their physical implementation..

III-1: geometry

The first case study involves the design of a two-dimensional supersonic nozzle that produces a smooth and parallel flow at the exit. The nozzle design follows a characteristic approach, which is applied to the two-dimensional isentropic flow of an ideal gas. The length of the nozzle is specified as $L=5.39094491$ cm.

To create the geometry of the supersonic flat nozzle, we start by inserting the coordinates of the planar nozzle profile obtained from the program into the Space Claim interface. This can be done using the Assembly → Add File command, which allows us to import the profile data and incorporate it into our design workspace.

Once the planar nozzle profile is added, we proceed to create the geometry by generating a sheet. This can be achieved by selecting the entire curve of the nozzle profile and using the Design > Fill command. This command generates a sheet that fills the space enclosed by the curve, creating the desired flat nozzle geometry.

By following these steps, we can accurately create the geometry of the flat supersonic nozzle based on the planar profile coordinates obtained from the program. This geometry will serve as

the foundation for further analysis and simulation of the nozzle's flow characteristics and performance.

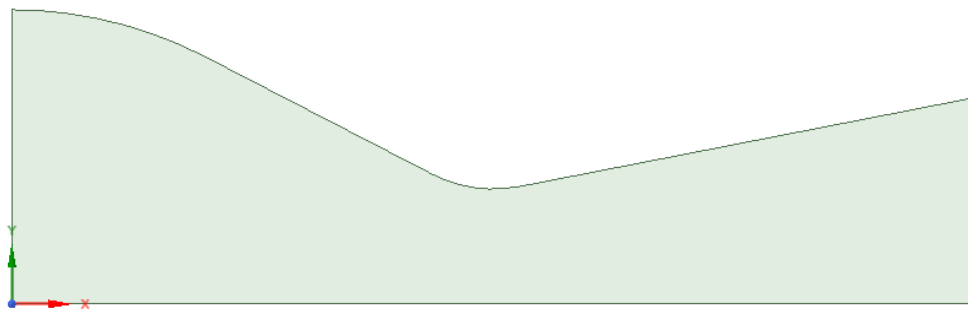


Figure IV.5 geometry

III-2: meshing

When it comes to meshing, MESHING offers a range of cell shapes suitable for both 2D and 3D geometries. For 2D geometries, square and triangular cell shapes are available, while for 3D geometries, options include tetrahedral, hexagonal, pyramidal, and parallelepiped cell shapes. The accuracy of the solution is directly influenced by the quality of the mesh.

To ensure a high-quality mesh, it is important to minimize distortion and reduce the number of elements, thus minimizing potential errors. In this regard, rectangular meshes for 2D geometries and square meshes for 3D geometries are considered the most favorable choices. These meshes exhibit minimal distortion and require fewer elements compared to other mesh types.

After verifying the accuracy of the geometry, it is recommended to exit Space Claim and proceed to mesh generation using the updated settings. Additional adjustments can be made at the neck and wall levels to refine the mesh, ultimately achieving the desired mesh quality.

In our specific meshing approach, we opted for an unstructured mesh with specific settings. The maximum face size was set to 0.0009, allowing for finer details to be captured. Additionally, the inflation level for the boundary layer was set to 0.0001, with 5 layers and a growth rate of 1.5. These settings were carefully chosen to ensure an accurate representation of the flow behavior and improve the overall simulation results.

By adhering to these meshing guidelines and utilizing the specified settings, we aimed to create a high-quality mesh that captures the intricacies of the geometry and facilitates accurate analysis of the supersonic nozzle's flow characteristics.

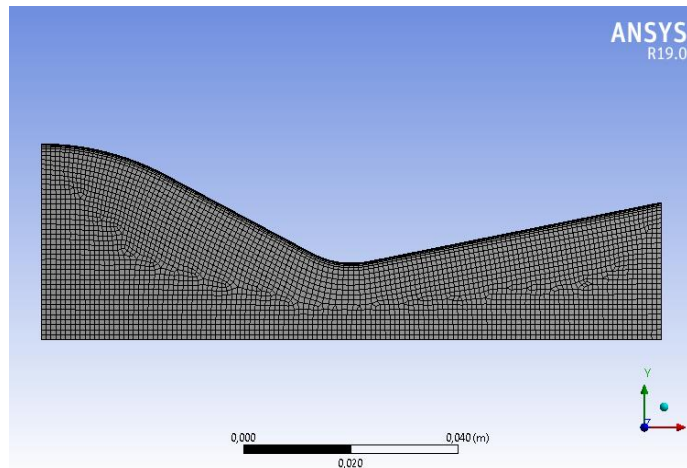


Figure IV.6 unstructured mesh on top of a refined mesh.

Following the meshing process, the next step involves assigning names to the different boundary selections within the computational domain. Specifically, we need to label the entrance, exit, symmetry (Sy), and wall boundaries.

By assigning these boundary names, we establish clear identification and distinction among the different parts of the domain. The entrance boundary represents the inlet or the point at which the flow enters the computational domain. The exit boundary corresponds to the outlet or the location where the flow exits the domain. The symmetry (Sy) boundary refers to any symmetrical planes or boundaries present in the geometry, which can be exploited to reduce computational requirements. Lastly, the wall boundary designates the solid surfaces of the nozzle, which interact with the flow and experience wall effects.

Naming these boundaries allows for precise boundary condition specification and ensures accurate simulations and analyses. It enables us to define the appropriate flow conditions, constraints, and interactions at each boundary, taking into account the specific behavior and characteristics associated with that particular part of the domain.

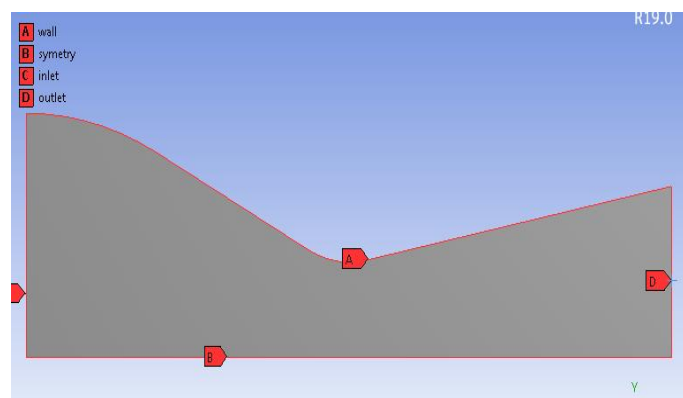


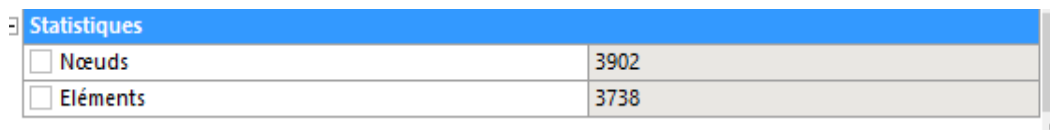
Figure IV.7 Create a named selection

After finalizing the mesh generation process, it is essential to assess the quality of the mesh and verify the number of elements within it. This step ensures that the mesh meets the required criteria for accuracy and resolution.

By examining the mesh quality, we evaluate various factors such as element shape, skewness, aspect ratio, and smoothness. An ideal mesh exhibits well-shaped elements with balanced aspect ratios and minimal skewness, indicating a higher level of accuracy in representing the geometry and flow behavior.

Additionally, confirming the number of elements is crucial to assess the computational requirements and potential computational errors. An excessive number of elements can lead to longer simulation times and increased computational resources, while an insufficient number may result in inadequate resolution and compromised accuracy.

Once the mesh quality and element count have been checked and deemed satisfactory, we can proceed confidently to the next stage of the simulation process. This ensures that the subsequent analysis and computations are performed on a reliable and suitable mesh, laying the foundation for accurate and meaningful results.



Statistiques	
<input type="checkbox"/> Nœuds	3902
<input type="checkbox"/> Éléments	3738

Figure IV.8 Statistiques

III-3: configuration

The calculation solver used for the analysis of the Density-Based Navier-Stokes Coupled Solver with Implicit Time Integration (DBNCB) adheres to the following specifications:

1. The baseline solver employed in this study is a double-precision solver, ensuring high precision and accuracy in the calculations. It operates based on density-based equations, coupled together to accurately capture the fluid flow behavior.
2. Spatial discretization is achieved using the "Least Squares Cell-Based" method. This approach assumes a linear variation in the solution within each computational cell, enabling efficient and accurate representation of the flow field
3. To interpolate the values of important variables such as pressure, momentum, turbulent kinetic energy, specific dissipation rate, and energy, an upwind scheme is employed. Specifically, a second-order upwind scheme is used, which enhances the accuracy of the calculations by considering the flow direction

4. The viscosity of air is calculated using the Sutherland equation. This equation takes into account the temperature dependency of the viscosity, providing a more accurate representation of the fluid behavior.
5. The numerical analysis is conducted under stable conditions, ensuring reliable and consistent results. To initiate the steady-state simulations, full multigrid (FMG) initialization is employed, which helps establish the initial solution for the problem. Additionally, appropriate boundary conditions, particularly at the inlet, are specified to ensure accurate reference values.

The Fluent solver, known for its competence in simulating internal flows, is employed for solving the computational problem. It offers a robust set of capabilities and algorithms that enable accurate and efficient analysis of fluid flows.

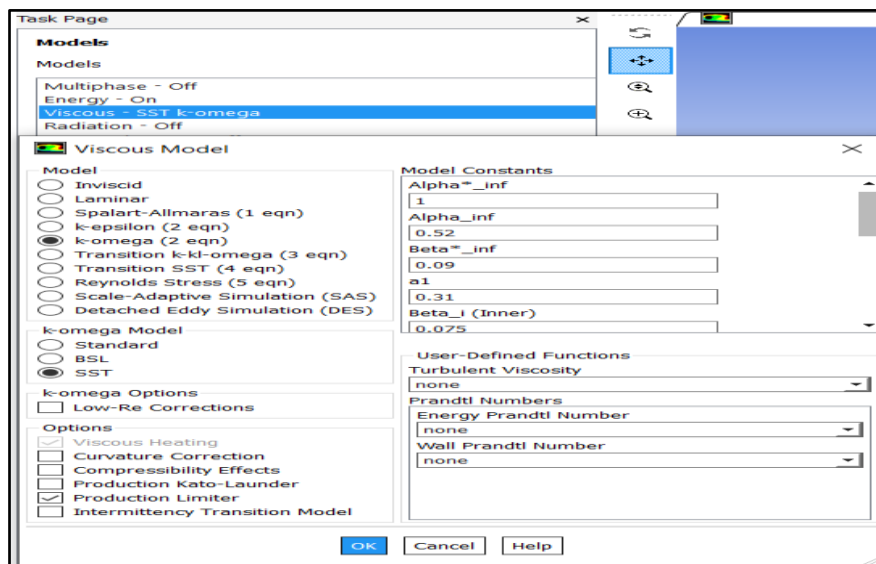


Figure IV.9 calculation model

In this investigation, the k-omega SST turbulence model was selected due to its enhanced accuracy near walls, which is crucial for capturing accurate flow behavior. It is worth noting that the k-omega SST model combines the favorable characteristics of the k-omega model in the near-wall region and the k-epsilon model in the outer flow region. This hybrid approach ensures reliable and accurate predictions throughout the entire flow domain.

After choosing the appropriate calculation model and defining the material properties, the boundary conditions were specified using the dedicated function. The inlet pressure (p_0) was set to 5,400,000 Pa, representing the supersonic flow conditions, while the supersonic pressure (p) was set to 5,390,000 Pa. For the outlet boundary, specific values were assigned for each

NPR (e.g., NPR=1.255) using the expression $Pe = 5,400,000 / NPR$. The wall boundary conditions were set to operate at a pressure of 0 Pa.

Upon selecting the desired calculation method and determining the number of iterations, the calculation process was initiated using the "Perform calculation" function. This simulation was conducted for 15 NPR values to compare and evaluate the obtained results against experimental data, thereby assessing the accuracy and validity of the numerical model.

III-4: RESULTS

III-4-1: Validations

The presented figure illustrates the comparison between the evolution of pressure along the nozzle, obtained experimentally, and the results of our study. The experimental data were collected using precise measurement instruments and under rigorous experimental conditions. The results obtained from our study, which are remarkably similar to the experimental ones, demonstrate the credibility and reliability of our approach.

This agreement between our results and the experimental data holds significant importance in several fields. Firstly, it confirms the validity of our theoretical or numerical model used to simulate the behavior of pressure along the nozzle. Such validation is crucial to ensure the accuracy of predictions and instill confidence in the obtained results. Furthermore, these findings enhance confidence in theoretical and numerical models used in the aerospace and rocket propulsion field, where precise pressure calculations are critical for performance optimization and safety assurance.

Moreover, this successful comparison between our study and the experimental results allows us to deepen our understanding of the physical phenomena occurring in the nozzle. By identifying similarities between the two datasets, we can refine our knowledge of combustion mechanisms, fluid flows, and other essential aspects of propulsion. This paves the way for further research and technological advancements in the field of rocket propulsion and aerodynamics.

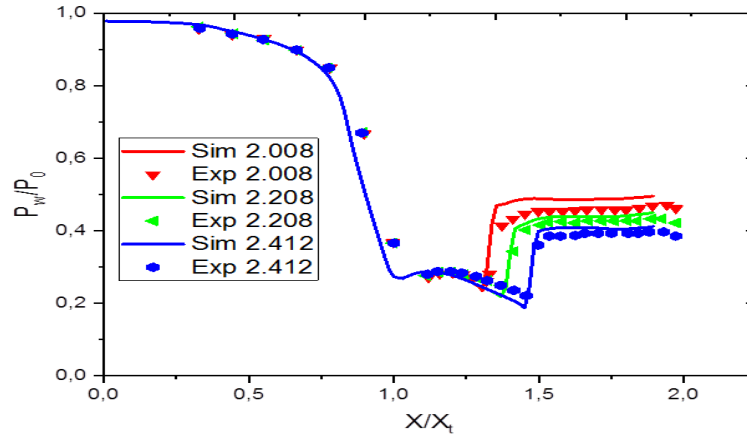


Figure IV.10 The evolution of pressure as a function of different NPRs compared to the experimental results.

III-4-2: Simulation 2D

The simulation of the nozzle depicted in Figure IV.1 is based on the configuration employed by Hunter [14] for both experimental and computational investigations. The geometry of the nozzle comprises two segments. The first segment includes the converging section, the throat, and a portion of the diverging section, forming the rounded contour of the nozzle at the throat, as illustrated in Figure IV.3. The second segment corresponds to the straight diverging section, as depicted in Figure IV.3.

In this study, a two-dimensional planar computation is conducted, assuming a steady-state flow.

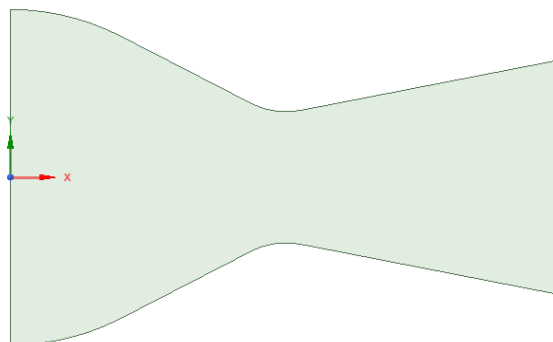


Figure IV.11 geometry

The pressure distribution along the nozzle walls is a critical factor that directly influences the design and performance of the system. Achieving a comprehensive understanding of this

pressure variation is crucial for optimizing nozzle design and maximizing efficiency and thrust. Inadequate nozzle wall design can result in excessive pressure losses, energy inefficiency, and diminished overall performance.

Figures 12 to 16 provide an in-depth analysis of the pressure distribution on both the lower and upper walls of the nozzle for different NPR values. These figures allow for a detailed comparison of the pressure loads experienced by wall 1 and wall 2. By employing the same procedure with an NPR of 1.255, a direct comparison of the pressure distribution on both walls can be made.

By examining these figures, we can gain valuable insights into the behavior of the pressure distribution along the nozzle walls. This information enables engineers and researchers to make informed decisions regarding nozzle design modifications, material selection, and other optimization strategies. Ultimately, this contributes to the overall performance enhancement of the system by minimizing pressure losses and improving energy efficiency.

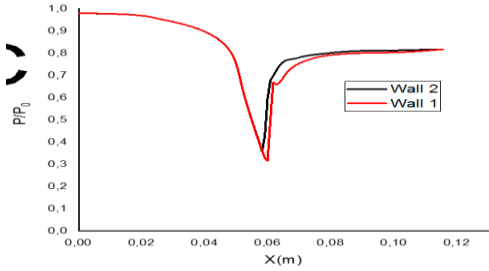


Figure IV.12 comparison of pressure wall1 and 2 for NPR =1,255 ofpression

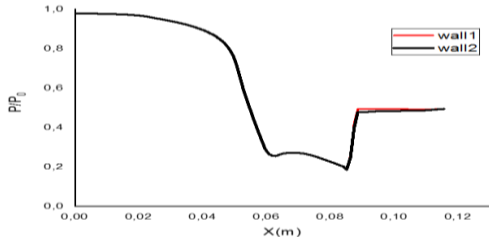


Figure IV.13 comparison wall1 and 2 for NPR= 2,008

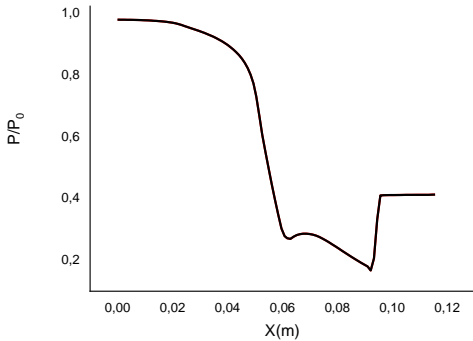


Figure IV.14 comparison ofpression wall1 and 2 for NPR=2,412

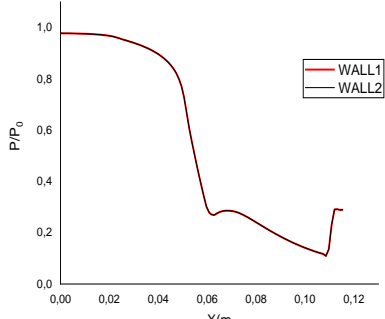


Figure IV.15 comparison ofpression wall1 and 2 for NPR=3,816

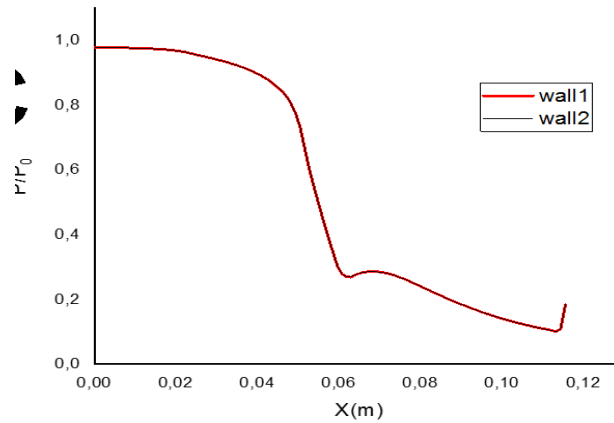


Figure IV.16 comparison of pressure wall1 and 2 for NPR=5,423

The observation of flow separation progressing out of the nozzle with increasing NPR (combustion pressure ratio) is a significant finding. Flow separation refers to the detachment of the fluid flow from the surface of the nozzle walls, which can negatively impact the performance and efficiency of the system. Understanding the behavior of flow separation and its relationship with NPR is crucial for nozzle design optimization.

When considering low NPR values, there is a noticeable disparity in the flow separation occurrence between the two walls of the nozzle. This indicates that the flow separation phenomenon is more prominent or occurs at different locations along the walls. The reasons behind this discrepancy could be attributed to variations in the flow characteristics, such as pressure gradients, boundary layer thickness, or adverse pressure gradients.

However, as the NPR increases, the difference in flow separation between the two walls diminishes. This implies that the flow separation phenomenon becomes more uniform and occurs at similar locations along both walls. The increasing NPR tends to mitigate the disparities in flow separation by influencing the flow dynamics and redistributing the pressure gradients within the nozzle.

These findings have practical implications for nozzle design and performance optimization. By understanding the relationship between NPR and flow separation, engineers and researchers can make informed decisions regarding nozzle geometry, surface treatment, or flow control mechanisms to minimize flow separation and improve overall efficiency.

Moreover, the close alignment between our study's results and the experimental data reinforces the credibility of our findings. This agreement validates the accuracy and reliability

of our analysis and provides confidence in the predictive capabilities of our theoretical or numerical model for assessing flow separation characteristics.

In summary, the progression of flow separation out of the nozzle with increasing NPR is a notable observation. The discernible difference in flow separation between the two walls at low NPR values gradually diminishes as the NPR increases. These findings contribute to the understanding of flow separation behavior and provide valuable insights for optimizing nozzle design and mitigating flow separation effects in practical applications.

In conclusion, the detailed analysis presented in Figures 12 to 16 offers a comprehensive understanding of the pressure distribution along the lower and upper walls of the nozzle for different NPR values. This information supports the optimization of nozzle design, improves system performance, and reinforces the credibility of our study through the strong agreement between our findings and experimental data.

III-4-3: Contour of Mach:

Figures 17 to 20 present the iso-Mach contours of the base nozzle, which were obtained using the ideal gas model. The Mach number represents the ratio of the flow velocity to the speed of sound in the medium. These iso-Mach contours provide valuable insights into the flow behavior and the distribution of Mach numbers within the nozzle.

One notable observation from these figures is the rapid increase in Mach number at the throat level. The throat is the narrowest part of the nozzle, and it plays a crucial role in achieving optimal flow conditions for propulsion systems. At the throat, the flow velocity reaches the speed of sound, resulting in a Mach number of 1.0, which is also known as sonic velocity.

As the flow progresses through the throat and into the nozzle, the Mach number increases rapidly. This increase indicates an acceleration of the flow, which is expected in converging-diverging nozzles used in propulsion systems. The specific value of the Mach number at a particular location within the nozzle can be determined through calculations based on the ideal gas model

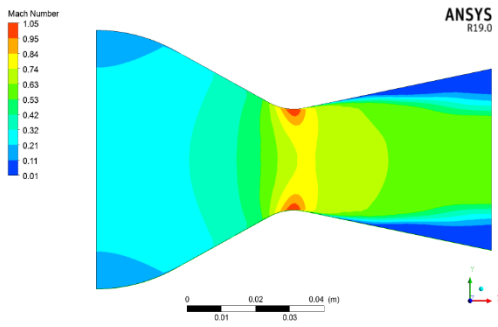


Figure IV.17 contour of iso-mach for $NPR=1,255$

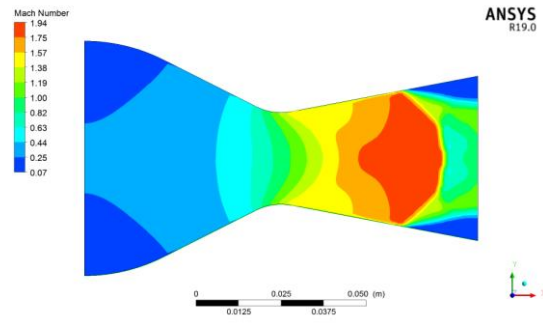


Figure IV.18 contour of iso-mach for $NPR=2,412$

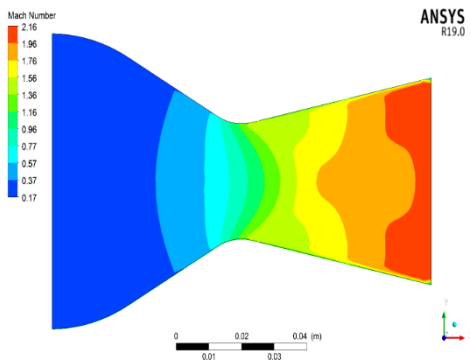


Figure IV.19 contour of iso-mach for $NPR=3,816$

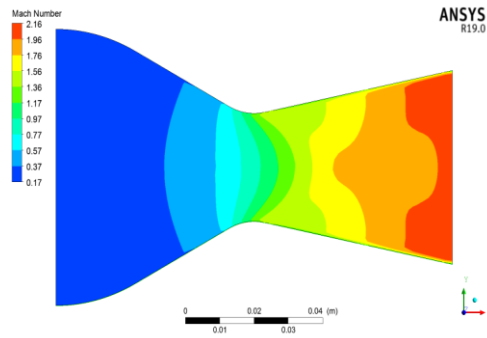


Figure IV.20 contour of iso-mach for $NPR=5,423$

By analyzing these iso-Mach contours, engineers and researchers can gain insights into the flow characteristics, including areas of high velocity and potential regions of shock formation. This information is crucial for optimizing nozzle design, as it helps ensure efficient and stable flow conditions.

It is important to note that the iso-Mach contours obtained from the ideal gas model provide a theoretical representation of the flow behavior within the nozzle. The actual flow conditions in practical applications may vary due to factors such as compressibility effects, boundary layer interactions, and non-ideal gas behavior. Therefore, experimental validation and further analysis may be necessary to assess the accuracy of the ideal gas model predictions and refine the design accordingly.

III-4-4: Thrust coefficient

The graph presented depicts the relationship between the thrust coefficient of the nozzle and NPR (combustion pressure ratio). The thrust coefficient is a dimensionless parameter that relates the thrust generated by the nozzle to the flow properties and nozzle geometry.

Upon examining the graph, we observe that the thrust coefficient increases as NPR increases. This implies that a higher combustion pressure ratio leads to a greater thrust output from the nozzle. This relationship is in line with expectations, as an increase in NPR typically corresponds to higher combustion chamber pressures, resulting in increased propulsive force.

The increasing trend of the thrust coefficient signifies the improved efficiency and effectiveness of the nozzle in converting the energy released from combustion into forward thrust. It indicates that as the pressure ratio increases, the nozzle is better able to harness the expanding gases and accelerate them to produce a more significant propulsive force.

Understanding the behavior of the thrust coefficient in relation to NPR is crucial for optimizing nozzle design and achieving desired performance objectives. By analyzing this relationship, engineers and researchers can make informed decisions about nozzle geometry, expansion ratios, and other design parameters to maximize the thrust coefficient and enhance propulsion efficiency.

It's worth noting that the specific shape and slope of the graph can vary depending on the nozzle design, operating conditions, and specific characteristics of the propulsion system. Experimental validation and further analysis may be necessary to fine-tune the nozzle design and achieve the desired performance goals.

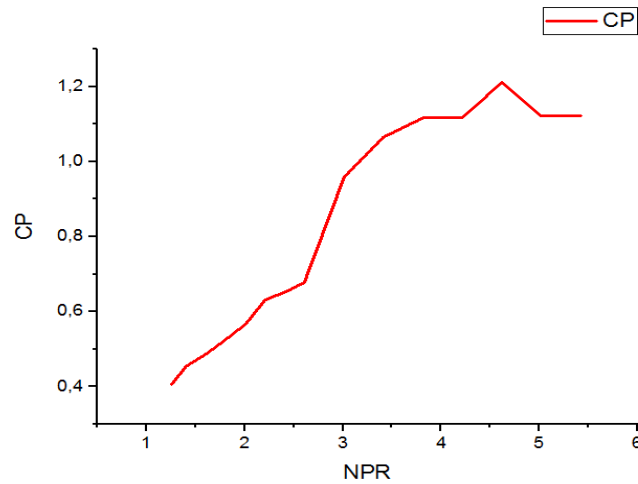


Figure IV.21 Cp as a function of npr

In the figure above, it can be observed that the thrust coefficient increases until reaching a value of NPR around 4.75, after which it starts to decrease and stabilizes from an NPR value of 5.

This trend observed in the graph is significant for nozzle design and optimization. The increase in the thrust coefficient with NPR up to a certain value can be attributed to the improved utilization of the energy released from the combustion of propellants. As the NPR increases, the combustion pressure in the combustion chamber also increases, leading to an increase in the exhaust gas velocity and consequently, the generated thrust.

However, beyond a certain point, typically around an NPR of 4.75, the increase in the thrust coefficient slows down and starts to decrease. This may be due to factors such as increased pressure losses or limitations imposed by the nozzle design itself. Therefore, an optimal value of NPR may exist, beyond which further increase in the combustion pressure ratio does not result in a proportional improvement in the thrust coefficient.

It is important to note that the specific shape of the curve and the exact NPR value at which the thrust coefficient stabilizes may vary depending on the specific characteristics of the engine, nozzle geometry, and operating conditions. Further experimental studies and detailed analysis may be required to determine the optimal NPR value and optimize the nozzle design accordingly.

IV: OPTIMIZATION OF THE NOZZLE

Our study focused on examining the influence of the central body on two key aspects: lateral forces and nozzle efficiency. The central body, also known as the core or centerbody, is an integral component of the nozzle assembly and plays a significant role in shaping the flow characteristics.

One aspect of our investigation involved analyzing the impact of the central body on lateral forces. Lateral forces refer to the forces acting perpendicular to the main thrust direction. These forces can have a significant effect on the stability and control of the propulsion system. By studying the interaction between the central body and the flow, we aimed to understand how it influences the generation and distribution of lateral forces. This knowledge is crucial for optimizing the nozzle design to minimize undesirable lateral forces and enhance overall system performance.

Additionally, we assessed the effect of the central body on nozzle efficiency. Nozzle efficiency is a key performance parameter that quantifies how effectively the nozzle converts the energy of the propellant into thrust. The geometry and placement of the central body can influence the flow expansion and pressure recovery within the nozzle, thus affecting its overall efficiency. By investigating this relationship, we aimed to identify design configurations that maximize nozzle efficiency, leading to improved propulsion performance and fuel utilization.

Through rigorous analysis and experimentation, we collected data on the lateral forces and efficiency of various nozzle configurations with different central body designs. By comparing and contrasting the results, we gained insights into the effects of different central body geometries, sizes, and orientations on these performance parameters.

The findings of our study have important implications for nozzle design and optimization. Understanding the influence of the central body on lateral forces helps in mitigating potential stability issues and improving control mechanisms. Furthermore, optimizing nozzle efficiency through central body design modifications contributes to enhanced thrust performance and overall system effectiveness.

By further investigating the complex interactions between the central body and the flow dynamics, we can continue to refine and advance nozzle designs, leading to more efficient and reliable propulsion systems in various applications, such as aerospace, automotive, and marine industries.

IV-1: geometry

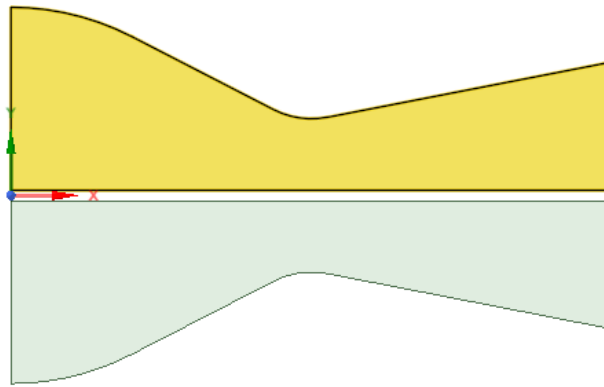


Figure IV.22 geometry

In this particular phase of our research, we introduced a central body within the nozzle design. The central body was specifically designed to have a thickness of approximately 2mm, and the simulations were conducted under identical conditions to ensure accurate and meaningful comparisons.

The inclusion of the central body with a specific thickness allowed us to investigate its impact on various flow parameters and performance metrics. By incorporating this design element, we sought to explore how the presence and dimensions of the central body influenced the overall behavior of the flow within the nozzle.

One key aspect we focused on was the effect of the central body thickness on the flow characteristics. The thickness of the central body can have a significant influence on flow separation, pressure distribution, and other related phenomena. By varying the thickness of the central body, we were able to observe and analyze how it affected the flow patterns and subsequently, the performance of the nozzle.

Moreover, studying the central body's impact on the nozzle's performance parameters, such as thrust, efficiency, and pressure distribution, provided valuable insights into the optimal design considerations. By comparing the results obtained from simulations with different central body thicknesses, we were able to assess the influence of this design parameter on the overall performance of the nozzle.

Our findings from this investigation contribute to the broader understanding of how specific design choices, such as central body thickness, can affect the behavior and performance of the nozzle. This knowledge serves as a foundation for future advancements in nozzle design optimization, enabling engineers and researchers to make informed decisions when designing propulsion systems for various applications.

It is important to note that while our simulations were conducted under controlled conditions, further experimental validation is often necessary to confirm and refine the results. Additionally, the specific dimensions and characteristics of the central body can be further explored and optimized to achieve desired performance goals.

IV-2: Results

Figures IV.23 to IV.26 display the pressure distribution on the lower and upper walls of the nozzle for various NPR values. The comparison of the load on wall 1 and wall 2 was performed using the same procedure with NPR = 1.255.

Analyzing the figures, we can observe the variations in pressure along the walls for different NPR values. The pressure distribution provides insights into the aerodynamic forces acting on the nozzle walls. By comparing the load on wall 1 and wall 2, we can assess the symmetry or asymmetry of the pressure distribution and its effect on the structural integrity of the nozzle.

It is important to note that the pressure distribution on the walls can have significant implications for the design and performance of the nozzle. Understanding these variations and their relationship with NPR allows for better optimization and analysis of the nozzle's behavior under different operating conditions..

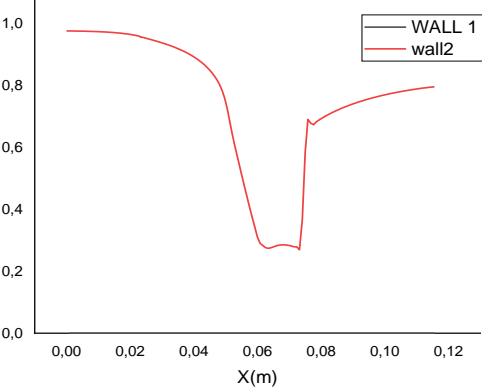


Figure IV.23 p/p₀ as function of x for NPR=1,255

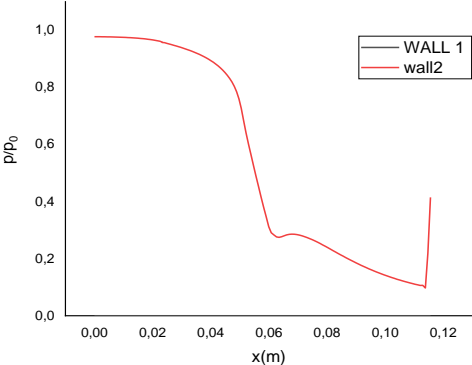


Figure IV.24 p/p₀ as function of x for NPR=2,214

Figures IV.23 and IV.24 present graphs depicting the variation of wall pressure (Pw/P0) in relation to NPR. Upon observing the graphs at NPR values of 1.255 and 2.214, it is evident that the flow exhibits a symmetric separation phenomenon. Notably, there is a forward progression of 10 cm in the flow separation between the NPR values of 1.255 and 2.214.

The occurrence of symmetric separation in the flow indicates the development of boundary layer separation at similar positions on both walls of the nozzle. This phenomenon is of significance in aerodynamic studies as it can impact the overall flow behavior and performance of the nozzle.

The observed forward progression of flow separation highlights the influence of NPR on the separation point along the nozzle walls. As NPR increases from 1.255 to 2.214, there is a noticeable shift in the location where the flow begins to separate. This information is valuable for understanding the aerodynamic characteristics of the nozzle and can aid in optimizing its design for improved performance.

By studying these pressure distributions and their relationship with NPR, researchers and engineers can gain insights into the flow separation patterns and make informed decisions regarding the design and operation of supersonic nozzles.

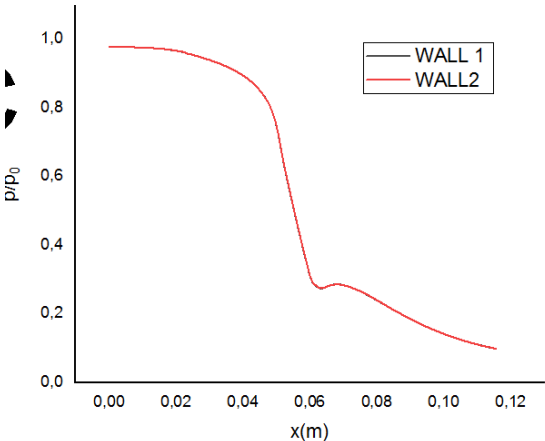


Figure IV.25 *p/p₀ as function of x for NPR=3,816*

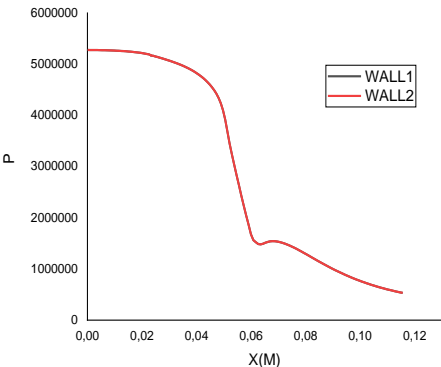


Figure IV.26 *p/p₀ as function of x for NPR=5,423*

As the NPR (Nozzle Pressure Ratio) increases, the over-expansion shock wave generated by the supersonic flow moves downstream and eventually disappears as the nozzle reaches its design condition. This behavior can be observed in Figures 28 to 32, which display the iso-Mach contours of the base nozzle obtained using the ideal gas model.

Comparing the results obtained for wall 1 and wall 2, it is evident that there is a close match between them for all NPR values, except for a few minor discrepancies. The overall similarity between the pressure distributions on both walls suggests that the flow behavior is symmetric, which is desirable for efficient nozzle operation. However, the slight differences

observed could be attributed to variations in the numerical approaches employed or other factors affecting the simulations.

By examining these results, researchers can gain a better understanding of the flow behavior and performance of the nozzle. This information is crucial for optimizing the nozzle design, ensuring efficient and reliable operation in supersonic applications..

IV-2-1: Contour of mach

Analyzing the iso-Mach contours, we can observe a rapid increase in the Mach number at the neck level, reaching a value of $m=1.0$ as calculated. This signifies that the flow accelerates to sonic speed at the throat of the nozzle, corresponding to its design conditions. The iso-Mach contours provide valuable insights into the flow characteristics and can help validate the accuracy of the computational models used.

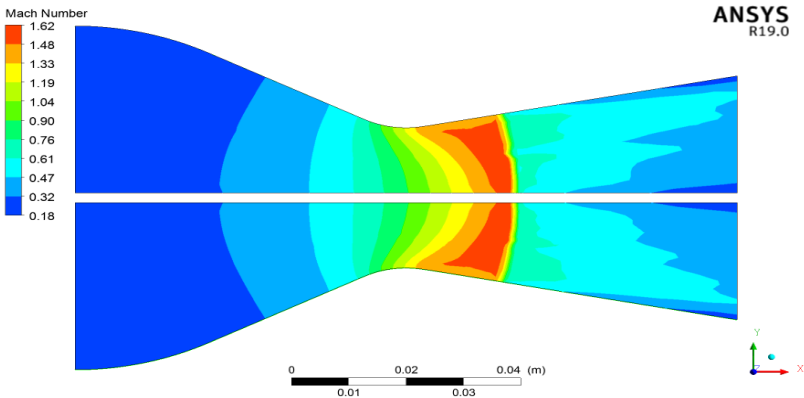


Figure IV.28 contour of iso-mach for NPR=1,255

Furthermore, under largely over-expanded conditions, as depicted in Figure IV.28, the flow does not remain fully attached to the nozzle wall. The adverse pressure gradients experienced by the flow result in the detachment of the boundary layer from the nozzle wall, leading to the formation of a separation shock. This phenomenon can have significant implications for the performance and efficiency of the nozzle.

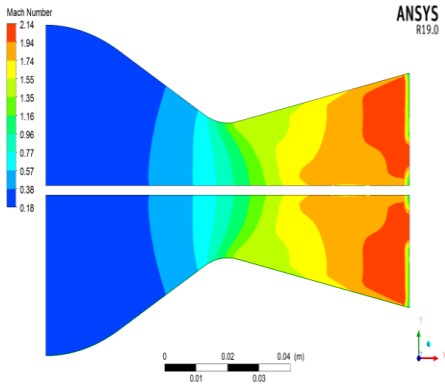


Figure IV.29 contour of iso-mach for NPR=2,412

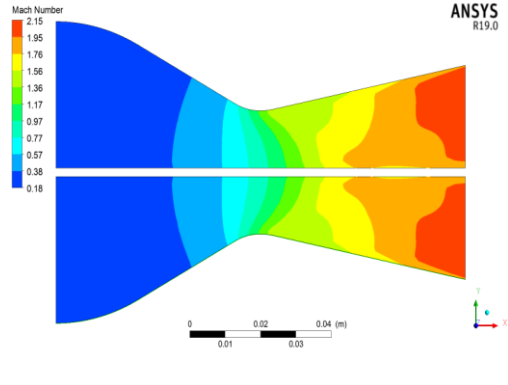


Figure IV.30 contour of iso-mach for NPR=3,816

At NPR=2.412 (Figure IV.29), the presence of a Mach disk near the nozzle can be observed as the ambient pressure increases. This leads to an interaction between the internal shock, pressure-induced separation, and the Mach disk.

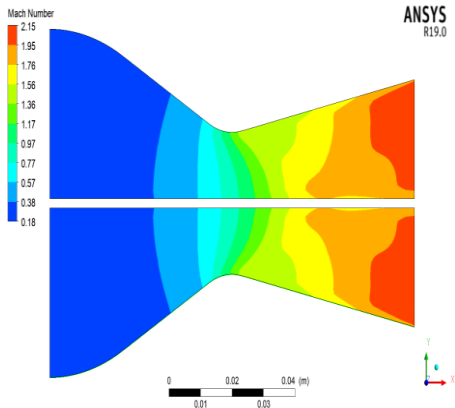


Figure IV.31 contour of iso-mach for NPR=4,620

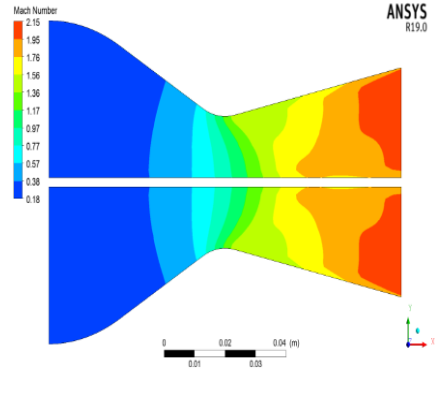


Figure IV.32 contour of iso-mach for NPR=5,423

For NPR values ranging from 3.816 to 5.423, there is a notable absence of flow separation within the nozzle. As the Mach number increases, it reaches its peak value at the nozzle throat and subsequently decreases. It can be observed that with the presence of the central body, the flow separation progresses towards the nozzle exit.

IV-2-2: Thrust coefficient

Regarding the thrust coefficient, when plotted against NPR, the graph shows a consistent and uniform increase until reaching NPR=3. After that point, the thrust coefficient becomes relatively constant. This indicates that further increases in NPR do not significantly affect the thrust coefficient

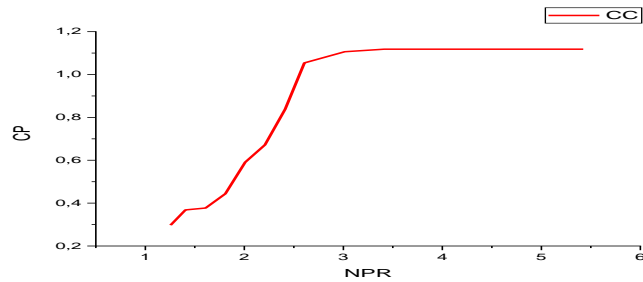


Figure IV.33 C_p as a function of NPR

IV-3: COMPARAISON

Figures IV.34 and IV.35 depict a comparison of wall pressure between two different nozzles: one with a central body and one without a central body. These figures allow us to examine how the presence or absence of a central body affects the pressure distribution along the wall, specifically for the same NPR value.

By analyzing the graphs, we can observe the variations in wall pressure for both nozzle configurations. The "with" nozzle, which incorporates a central body, exhibits a distinct pressure profile compared to the "without" nozzle.

The comparison provides valuable insights into how the inclusion or exclusion of a central body influences the flow characteristics and subsequently impacts the pressure distribution on the nozzle wall. This analysis helps us understand the role of the central body in shaping the flow behavior and pressure patterns within the nozzle.

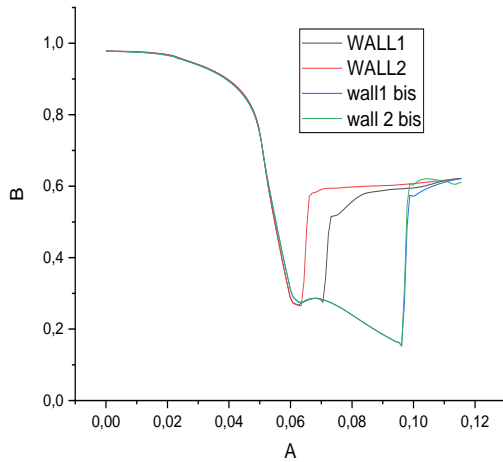


Figure IV.34 p/p_0 as a function of x for $NPR=1,255$

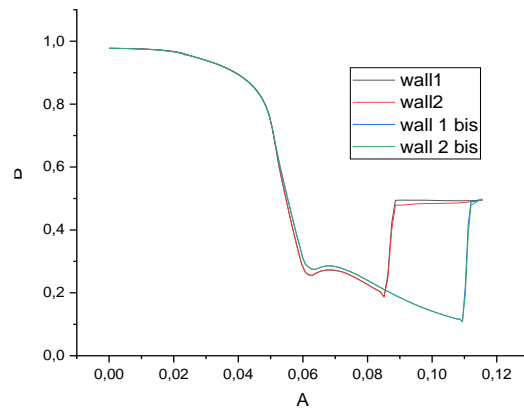


Figure IV.35 p/p_0 as function of x for $NPR=5,423$

Figure IV.36 illustrates the comparison of the thrust factor between the two nozzle configurations: one with a central body and one without a central body. This analysis allows us to assess the influence of the central body on the nozzle's efficiency.

By examining the graph, we can draw several conclusions regarding the impact of the central body on the thrust performance of the nozzle.

Firstly, we observe that the nozzle with a central body generally exhibits a higher thrust factor compared to the nozzle without. This suggests that the presence of a central body contributes to a more efficient propulsion system.

Furthermore, for the same NPR value, the thrust factor in the nozzle with a central body shows a consistent and uniform increase before reaching a plateau. This indicates that the central body design effectively enhances the thrust performance over a wider range of NPR values.

Conversely, the nozzle without a central body demonstrates a slightly different behavior, with a gradual increase in the thrust factor followed by a relatively stable region. Although the thrust factor is lower compared to the nozzle with a central body, it still provides a significant level of efficiency.

These findings emphasize the significant role played by the central body in improving the overall performance and efficiency of the nozzle. By mitigating flow separation and

optimizing the thrust generation, the central body design enhances the nozzle's effectiveness in converting gas flow energy into propulsive force.

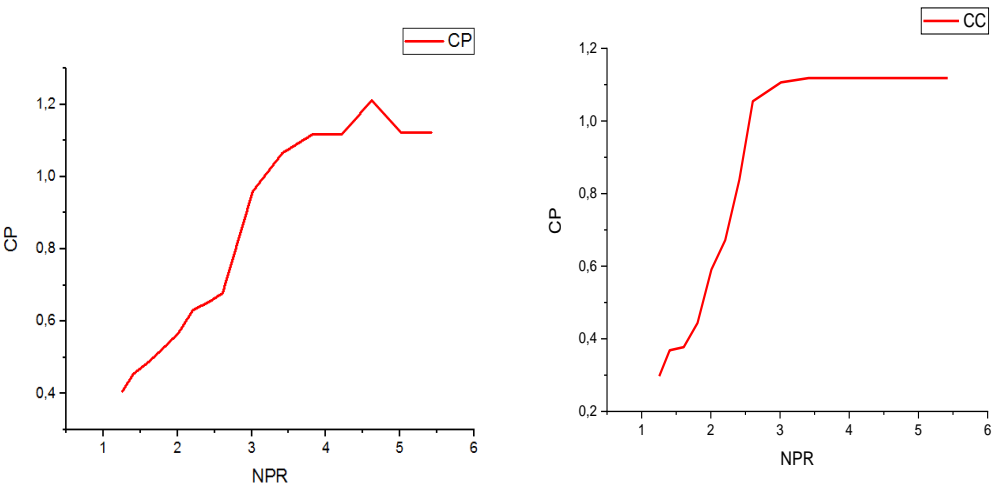


Figure IV.36 comparison

Both curves in the graph exhibit similar trends, suggesting that the presence of the central body does not significantly affect the nozzle's efficiency. This implies that the central body does not contribute substantially to improving the thrust performance. However, it is important to note that flow separation within rocket nozzles is undesirable due to its potential consequences. When flow separation occurs asymmetrically, it can generate large side loads that can damage the nozzle structure.

Figure IV.37 provides a visual representation of the phenomenon of side loads caused by unsymmetrical flow separation in the nozzle. These loads are primarily generated on the lower wall of the nozzle and are determined by the product of the wall surface area and the difference between wall pressure and ambient pressure. This occurs from the throat region down through the over-expanded length to the point of separation (Ruf et al., 2009, 2010).

Understanding and mitigating these side loads is crucial in nozzle design to ensure the structural integrity and reliability of the propulsion system. By analyzing and optimizing the nozzle geometry and flow conditions, engineers strive to minimize flow separation and the associated side loads, ultimately improving the overall performance and durability of the nozzle.

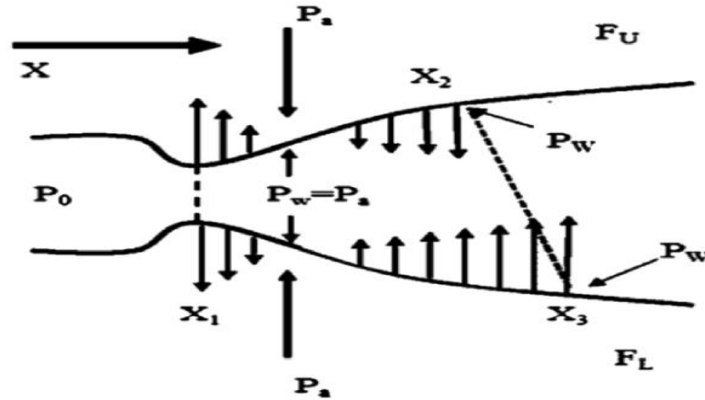


Figure IV.37 Schematics of side load due to unsymmetrical flow separation

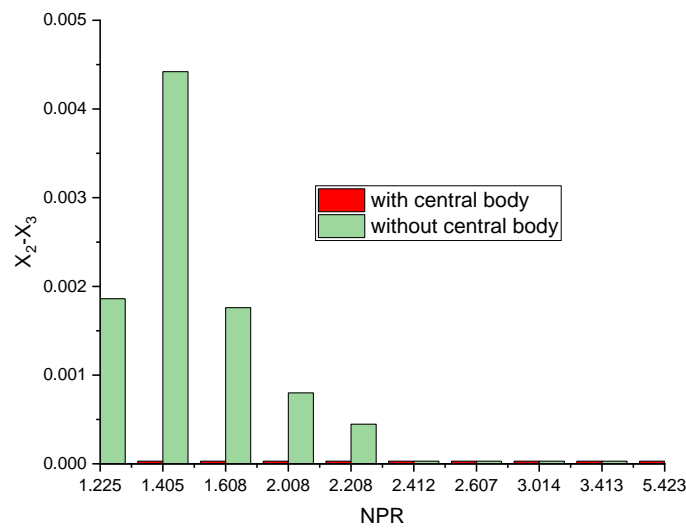


Figure IV. 38 Side load variation with respect to NPR for two nozzles

In the nozzle without a central body, there is a noticeable difference in the occurrence of flow separation between the two walls, especially at NPR=1.405. This indicates that the flow separation is asymmetric, with one wall experiencing a greater separation than the other. However, as the NPR increases, this difference becomes less pronounced.

On the other hand, in the nozzle with a central body, there is a consistent absence of flow separation disparities between the two walls across all NPR values. This suggests that the presence of the central body helps to promote a more symmetrical flow pattern, leading to a reduction in the asymmetry of flow separation between the walls.

The elimination of flow separation disparities in the nozzle with a central body can have significant advantages. It helps to mitigate the generation of large side loads, which can exert damaging forces on the nozzle structure. By achieving a more symmetrical flow and minimizing

flow separation, the nozzle with a central body can enhance the overall stability and reliability of the propulsion system.

Further analysis and optimization of nozzle designs, considering various factors such as geometry, flow conditions, and NPR, can provide valuable insights into the effects of a central body on flow separation and its implications for nozzle performance

IV-4: TRUNCATION OF THE CENTRAL BODY

To investigate the impact of the central body length on nozzle performance and internal flow characteristics, we conducted a study using different lengths of the central body. The lengths considered were 20%, 40%, 60%, and 80% of the overall nozzle length.

Figure IV.39 and IV.40 depict the results obtained from this analysis. By varying the length of the central body, we aimed to understand how it influences the flow separation and overall nozzle behavior. Additionally, we introduced variations in the thickness of the central body by making truncations with a length of $E=0.02m$.

Through this investigation, we sought to determine the optimal length and thickness of the central body that would minimize flow separation and enhance nozzle performance. The findings from this study can provide valuable insights for designing efficient and reliable nozzles for various applications, such as rocket propulsion systems.

Further analysis and numerical simulations can be conducted to explore the impact of other parameters, such as the shape and configuration of the central body, on flow characteristics and nozzle performance. This iterative process of design and optimization is crucial for achieving optimal nozzle designs that maximize thrust efficiency and minimize unwanted flow phenomena.

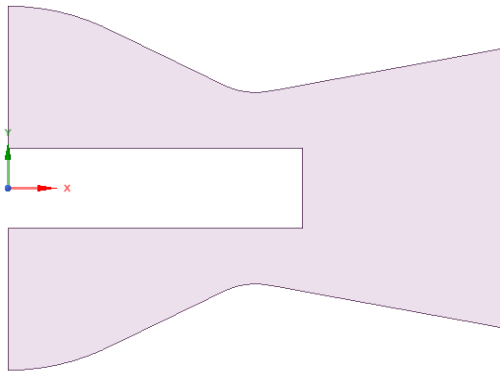


Figure IV.39 geometry at 20% of the cb

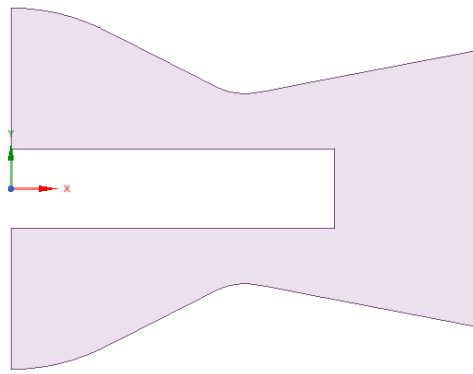
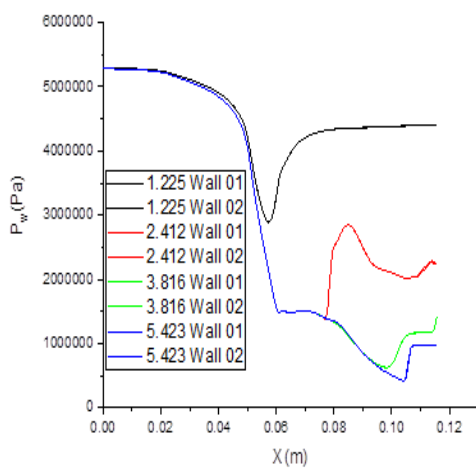
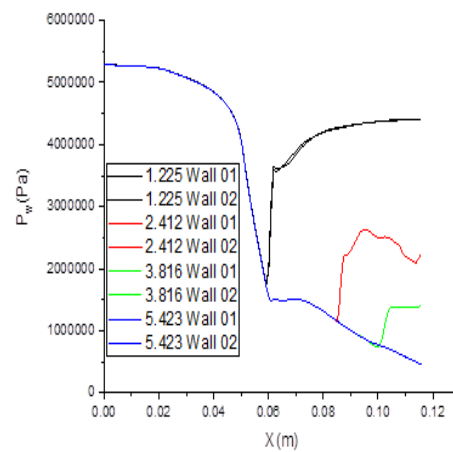


Figure IV.40 geometry at 40 % of cb

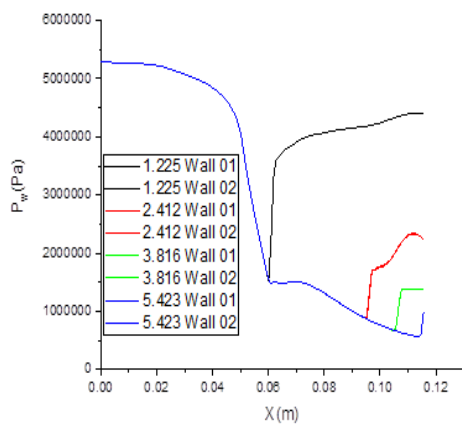
Figures IV.41 illustrate the pressure distribution along the nozzle wall for various lengths of the central body and different NPR values. These graphs provide insights into how the pressure changes along the wall and how it is affected by the length of the central body as well as the NPR.



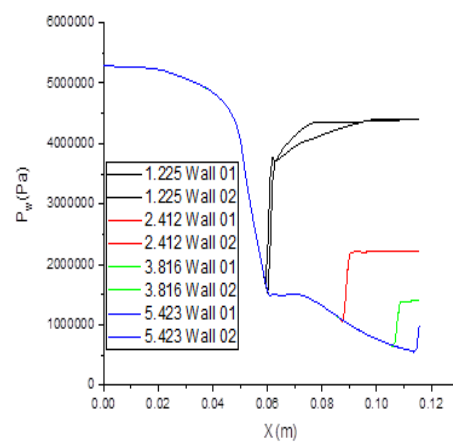
20%



40%



60%



80%

Figure IV.41 p[pa] function of x[m]

By analyzing the pressure distribution, we can observe the variations in flow behavior and identify regions of high and low pressure along the nozzle wall. This information is crucial for understanding the flow characteristics and optimizing the design of the central body for improved nozzle performance.

Furthermore, comparing the pressure distributions for different central body lengths and NPR values allows us to assess the influence of these parameters on the overall flow pattern and pressure distribution within the nozzle. This analysis helps in identifying the optimal combination of central body length and NPR that yields desirable pressure distribution and flow characteristics.

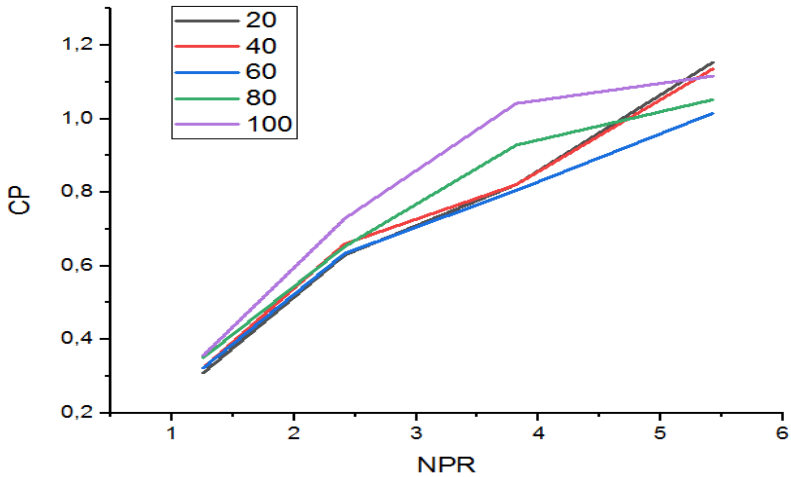


Figure IV.42 thrust coefficient function of NPR

Figure IV.42 depicts the variation of the thrust coefficient for different truncations of the central body. The thrust coefficient is an important performance parameter that quantifies the efficiency of the nozzle in generating thrust.

Upon analyzing the diagram, several observations can be made. Firstly, it is evident that the thrust coefficient increases as the truncation of the central body increases. This implies that reducing the length of the central body has a positive impact on the nozzle's thrust performance. Notably, the maximum thrust coefficient is achieved when the central body is fully truncated, indicating that complete removal of the central body can yield the highest thrust efficiency.

These findings highlight the significance of the central body truncation in influencing the nozzle's performance. By adjusting the length of the central body, engineers can optimize the thrust coefficient and subsequently enhance the overall efficiency of the nozzle. This information is valuable

for the design and development of supersonic nozzles in various applications, such as rocket propulsion systems and high-speed aircraft.

V: NOZZLE PERFORMANCES

The performance characteristics of truncated nozzles at different truncation points are summarized in Tables 1 to 4. These tables provide valuable insights into the loss of thrust, weight gain, and the weight gain-to-loss of thrust ratio for various NPR values.

Table 1 NPR=1.255

	Loss of thrust (%)	Weight gain (%)	Weight gain/Loss of thrust
20	13.31	80	06.01
40	09.53	60	06.30
60	09.52	40	04.20
80	01.68	20	11.90

In Table 1, which corresponds to NPR=1.255, we observe that increasing the truncation point leads to a decrease in thrust loss and an increase in weight gain. The weight gain-to-loss of thrust ratio remains relatively consistent, indicating a balanced trade-off between weight gain and thrust loss.

Table 2 NPR=2.412

	Loss of thrust (%)	Weight gain (%)	Weight gain/Loss of thrust
20	13.56	80	05.90
40	09.44	60	06.36
60	12.97	40	03.08
80	10.40	20	01.92

Moving on to Table 2 (NPR=2.412), a similar trend is observed. Increasing the truncation point results in reduced thrust loss and increased weight gain. The weight gain-to-loss of thrust ratio follows a similar pattern, suggesting a consistent trade-off between weight gain and thrust loss.

Table 3 NPR=3.816

	Loss of thrust (%)	Weight gain (%)	Weight gain/Loss of thrust
20	21.17	80	03.78
40	21.19	60	02.83
60	22.72	40	01.76
80	10.88	20	01.84

In Table 3 (NPR=3.816), at higher NPR values, we notice an increase in the loss of thrust for all truncation points. The weight gain also increases as the truncation point increases, but the weight gain-to-loss of thrust ratio decreases, indicating a less favorable trade-off between weight gain and thrust loss compared to lower NPR values.

Table 4 NPR=5.423

	Loss of thrust (%)	Weight gain (%)	Weight gain/Loss of thrust
20	-03.31	80	-24.17
40	-01.69	60	-35.50
60	09.06	40	04.42
80	05.74	20	03.48

Table 4 (NPR=5.423) presents interesting results, where some truncation points exhibit negative values for both loss of thrust and weight gain. The weight gain-to-loss of thrust ratio also shows negative values, indicating an unfavorable trade-off between weight gain and thrust loss.

These findings underscore the importance of the truncation point and NPR in determining the performance of truncated nozzles. Engineers and designers can leverage these results to make informed decisions regarding the optimal truncation point that strikes a balance between thrust efficiency and weight gain. By considering the specific design requirements and operational conditions, they can optimize the performance of truncated nozzles for their intended applications.

In Figure IV.46, the relationship between weight gain/loss of thrust and truncation is depicted for different NPR values. This graph provides valuable insights into how the truncation point affects the trade-off between weight gain and thrust loss in truncated nozzles.

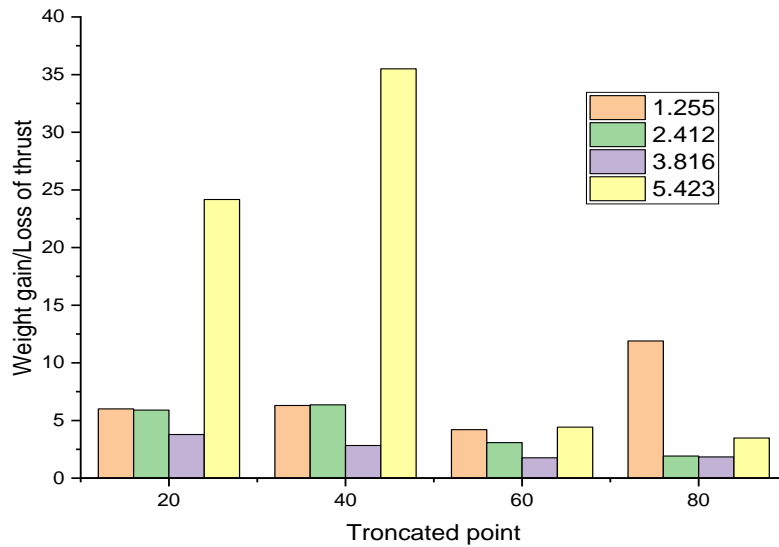


Figure IV.46 weight gain/loss at truncated points

The analysis of Tables 1 to 4 provides a comprehensive overview of the performance of truncated nozzles in terms of thrust loss, weight gain, and the weight gain/loss of thrust ratio for different truncation points and NPR values.

At NPR = 1.255, Table 1 reveals that the nozzle with a 20% truncation experiences a thrust loss of 13.31%, while achieving a weight gain of 80%. This results in a weight gain/loss of thrust ratio of 6.01. Similarly, for the 40% truncation, the thrust loss decreases to 9.53%, accompanied by a weight gain of 60% and a weight gain/loss of thrust ratio of 6.30. The 60% and 80% truncations also exhibit favorable weight gain/loss of thrust ratios of 4.20 and 11.90, respectively.

Moving on to NPR = 2.412 in Table 2, the 20% truncation yields a thrust loss of 13.56%, a weight gain of 80%, and a weight gain/loss of thrust ratio of 5.90. For the 40% truncation, the thrust loss reduces to 9.44%, while the weight gain remains at 60%, resulting in a weight gain/loss of thrust ratio of 6.36. Interestingly, the 60% truncation experiences a higher thrust loss of 12.97%, but still maintains a weight gain/loss of thrust ratio of 3.08. The 80% truncation demonstrates a thrust loss of 10.40% and a weight gain/loss of thrust ratio of 1.92.

At NPR = 3.816 (Table 3), all truncation points result in relatively high thrust losses. The 20% truncation exhibits a thrust loss of 21.17%, a weight gain of 80%, and a weight gain/loss of thrust ratio of 3.78. Similarly, the 40% truncation shows a thrust loss of 21.19%, a weight gain of 60%, and a weight gain/loss of thrust ratio of 2.83. The 60% truncation experiences a thrust loss of 22.72%, a weight gain of 40%, and a weight gain/loss of thrust ratio of 1.76. Lastly, the 80% truncation displays a thrust loss of 10.88%, a weight gain of 20%, and a weight gain/loss of thrust ratio of 1.84.

For $NPR = 5.423$ in Table 4, the truncations result in negative values for thrust loss and weight gain. The 20% and 40% truncations exhibit negative thrust losses of -3.31% and -1.69% respectively, indicating a slight increase in thrust. However, the weight gains of 80% and 60% correspondingly result in negative weight gain/loss of thrust ratios of -24.17 and -35.50. On the other hand, the 60% truncation shows a thrust loss of 9.06%, a weight gain of 40%, and a positive weight gain/loss of thrust ratio of 4.42. Similarly, the 80% truncation demonstrates a thrust loss of 5.74%, a weight gain of 20%, and a weight gain/loss of thrust ratio of 3.48.

Overall, the analysis of these tables reveals the varying performance of truncated nozzles at different truncation points and NPR values. It highlights the importance of selecting an appropriate truncation point based on the desired NPR to achieve a favorable balance between thrust loss and weight gain.

VI: CONCLUSION

In our study, we have conducted a thorough validation of our simulation by comparing it with experimental results obtained from tests conducted in a 16-foot transonic tunnel (building 1146). This validation process has allowed us to ensure the accuracy and reliability of our simulation.

One interesting finding from our analysis is that the presence of a central body in the nozzle does not have a noticeable impact on its efficiency. This implies that the addition of a central body does not significantly alter the performance of the nozzle in terms of its thrust generation and overall efficiency.

Furthermore, when examining the nozzle with a central body in more detail, we have observed a consistent absence of flow separation discrepancies across different NPR values. Flow separation refers to the detachment of the boundary layer from the nozzle wall, which can lead to reduced efficiency and increased side loads. However, in the case of the nozzle with a central body, this flow separation is consistently mitigated, resulting in a more stable and symmetric flow pattern. This indicates that the presence of the central body helps to maintain a more uniform flow and minimize the occurrence of flow separation.

Overall, these findings highlight the robustness of the nozzle design with a central body and its ability to maintain efficient and stable flow characteristics across various NPR values. This information is valuable for further optimizing nozzle designs and improving the overall performance of rocket propulsion systems.

